

## Accepted Manuscript

The isotopic composition and fluxes of particulate organic carbon exported from the eastern margin of the Tibetan Plateau

Jin Wang, Robert G. Hilton, Zhangdong Jin, Fei Zhang, Alexander L. Densmore, Darren R. Gröcke, Xiaomei Xu, Gen Li, A. Joshua West

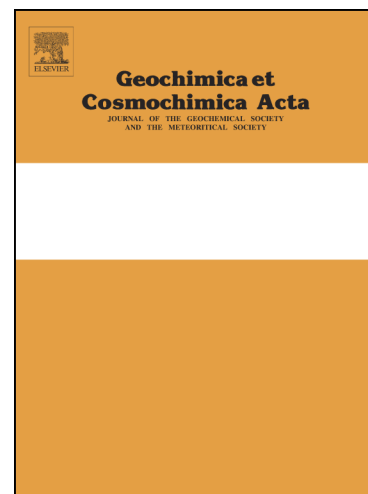
PII: S0016-7037(19)30116-4  
DOI: <https://doi.org/10.1016/j.gca.2019.02.031>  
Reference: GCA 11146

To appear in: *Geochimica et Cosmochimica Acta*

Received Date: 11 September 2018  
Revised Date: 15 February 2019  
Accepted Date: 15 February 2019

Please cite this article as: Wang, J., Hilton, R.G., Jin, Z., Zhang, F., Densmore, A.L., Gröcke, D.R., Xu, X., Li, G., Joshua West, A., The isotopic composition and fluxes of particulate organic carbon exported from the eastern margin of the Tibetan Plateau, *Geochimica et Cosmochimica Acta* (2019), doi: <https://doi.org/10.1016/j.gca.2019.02.031>

This is a PDF file of an unedited manuscript that has been accepted for publication. As a service to our customers we are providing this early version of the manuscript. The manuscript will undergo copyediting, typesetting, and review of the resulting proof before it is published in its final form. Please note that during the production process errors may be discovered which could affect the content, and all legal disclaimers that apply to the journal pertain.



# The isotopic composition and fluxes of particulate organic carbon exported from the eastern margin of the Tibetan Plateau

Jin Wang<sup>a,b</sup>, Robert G. Hilton<sup>b</sup>, Zhangdong Jin<sup>a,c,d,\*</sup>, Fei Zhang<sup>a</sup>, Alexander L. Densmore<sup>b</sup>, Darren R. Gröcke<sup>e</sup>, Xiaomei Xu<sup>f</sup>, Gen Li<sup>g</sup>, A. Joshua West<sup>g</sup>

<sup>a</sup> State Key Laboratory of Loess and Quaternary Geology, Institute of Earth Environment, Chinese Academy of Sciences, Xi'an, 710061, China

<sup>b</sup> Department of Geography and Institute of Hazard, Risk and Resilience, Durham University, Durham, DH1 3LE, UK

<sup>c</sup> CAS Center for Excellence in Quaternary Science and Global Change, Xian 710061, China

<sup>d</sup> Institute of Global Environmental Change, Xi'an Jiaotong University, Xi'an 710049, China

<sup>e</sup> Department of Earth Sciences, Durham University, Durham, DH1 3LE, UK

<sup>f</sup> Department of Earth System Science, University of California, Irvine, Irvine, CA 92697-3100, USA

<sup>g</sup> Department of Earth Sciences, University of Southern California, Los Angeles, California 90089, USA

Corresponding author at: SKLLQG, Institute of Earth Environment, Chinese Academy of Sciences, Xi'an, 710061, China

E-mail address: zhdjin@ieecas.cn (Z. Jin).

## Abstract

Erosion of organic carbon from the terrestrial biosphere and sedimentary rocks plays an important role in the global carbon cycle across a range of timescales. Over geological timescales ( $>10^4$  years), erosion and burial of particulate organic carbon (POC) from the terrestrial biosphere ( $\text{POC}_{\text{biosphere}}$ ) is an important  $\text{CO}_2$  sink, while oxidation of organic carbon derived from sedimentary rocks (petrogenic,  $\text{POC}_{\text{petro}}$ ) releases  $\text{CO}_2$  to the atmosphere. Over decadal to millennial timescales, the balance between  $\text{POC}_{\text{biosphere}}$  production and degradation affects atmospheric  $\text{CO}_2$  concentrations. To better constrain the controls on erosional carbon transfers, here we quantify  $\text{POC}_{\text{biosphere}}$  and  $\text{POC}_{\text{petro}}$  fluxes in a mountain range with relatively low runoff, the Longmen Shan, which drains the eastern margin of the Tibetan Plateau. We measure total organic carbon content ( $[\text{OC}_{\text{total}}]$ ) and the carbon isotopic compositions ( $^{13}\text{C}/^{12}\text{C}$  expressed as  $\delta^{13}\text{C}$ ;  $^{14}\text{C}/^{12}\text{C}$  expressed as fraction modern or  $F_{\text{mod}}$ ) of organic matter in suspended sediments collected from six gauging stations on the Min Jiang, a tributary of the Yangtze River, from 2005 to 2012. We find that  $\text{POC}_{\text{petro}}$  has a large range of  $\delta^{13}\text{C}$ , from  $-26.2\text{‰}$  to  $-13.2\text{‰}$ . This  $\text{POC}_{\text{petro}}$  mixes with

$\text{POC}_{\text{biosphere}}$  to set the  $\delta^{13}\text{C}$  of POC in river sediments. Binary mixing models reveal the possibility of aged  $\text{POC}_{\text{biosphere}}$  at two gauging stations which drain the high elevations of the eastern Tibetan Plateau, with modelled  $F_{\text{mod}}$  values of  $0.82 \pm 0.09$  and  $0.84 \pm 0.08$ . This is consistent with prior suggestions of aged biospheric carbon being eroded from the Plateau.

The annual  $\text{POC}_{\text{petro}}$  yields range from  $0.04 \pm 0.02 \text{ tC km}^{-2} \text{ yr}^{-1}$  to  $1.69 \pm 0.56 \text{ tC km}^{-2} \text{ yr}^{-1}$  across the five study catchments, with basin average yield that appears to be linked to catchment average slope as a likely proxy for erosion rate. Here, the variability in the petrogenic organic carbon content of rocks masks the signal of the weathering and oxidation of this rock-derived organic carbon. The annual  $\text{POC}_{\text{biosphere}}$  yields range from  $0.21 \pm 0.04 \text{ tC km}^{-2} \text{ yr}^{-1}$  to  $3.33 \pm 0.57 \text{ tC km}^{-2} \text{ yr}^{-1}$ . These values are towards the lower end of those measured in mountain ranges around the world, which we suggest not only reflects the relatively low erosion rates of the Longman Shan, but also the low annual runoff ( $<1 \text{ m yr}^{-1}$ ). Across this region, the river  $\text{POC}_{\text{biosphere}}$  discharge is related to the intensity of runoff events. Our data suggest that a wetter (and/or stormier) climate could increase the erosional export of  $\text{POC}_{\text{biosphere}}$  in this tectonically-active mountain range. Depending on the fate of  $\text{POC}_{\text{biosphere}}$  downstream in larger river systems, this could act as carbon-cycle climate feedback over geological timescales.

## 1. Introduction

Rivers play an important role in the global carbon cycle, exporting terrestrial carbon to the ocean and acting as biogeochemical reactors which can exchange carbon dioxide ( $\text{CO}_2$ ) with the atmosphere (Mayorga et al., 2005; Battin et al., 2008; Galy et al., 2015). Physical erosion in river catchments can mobilize particulate organic carbon from the terrestrial biosphere ( $\text{POC}_{\text{biosphere}}$ ) and from sedimentary rocks (petrogenic POC or  $\text{POC}_{\text{petro}}$ ) (Blair et al., 2003; Leithold et al., 2006; Galy et al., 2007; Hilton et al., 2008a). Erosion and transport of  $\text{POC}_{\text{biosphere}}$  and  $\text{POC}_{\text{petro}}$  can have different impacts on the atmospheric  $\text{CO}_2$  budget across a range of timescales (Galy et al., 2015; Hilton, 2017). Over geological timescales, erosion and burial of  $\text{POC}_{\text{biosphere}}$  is an important  $\text{CO}_2$  sink (Bernier, 1982; France-Lanord and Derry, 1997), while oxidation of  $\text{POC}_{\text{petro}}$  will release  $\text{CO}_2$  into the atmosphere (Petsch et al., 2000; Bouchez et al., 2010; Hilton et al., 2014; Hemingway et al., 2018). Over

shorter timescales (decades to millennia), the balance between  $\text{POC}_{\text{biosphere}}$  production and degradation may be large enough to influence atmospheric  $\text{CO}_2$  concentrations (Berhe et al., 2007; Yue et al., 2016).

Globally, physical erosion is thought to be the primary control on POC discharge by rivers (Galy et al., 2015; Hilton, 2017). Climate and tectonics are the two main factors governing the rates and patterns of physical erosion (Milliman and Farnsworth, 2011), therefore regulating POC discharge (Hilton, 2017). However, the relative roles of tectonic and climatic drivers of POC erosion – and thus the links between mountain building, the carbon cycle, and changes in climate – remain unresolved in many parts of the world. The India-Eurasia collision zone and high-elevation Tibetan Plateau are recognized for their important contributions to the global fluxes of fluvial sediments and solutes (Galy and France-Lanord, 2001; Milliman and Farnsworth, 2011). A large body of prior work has focused on the frontal Himalaya (France-Lanord and Derry, 1997; Galy et al., 2007, 2008a; Galy and Eglinton, 2011), where the rapid rates of tectonic uplift and associated physical erosion result in high POC yields (Galy et al., 2015). It is thought that more than 50% of  $\text{POC}_{\text{biosphere}}$  carried by the Ganges and Brahmaputra Rivers draining from the Himalaya is degraded and replaced by lowland-derived  $\text{POC}_{\text{biosphere}}$  during floodplain transit (Galy et al., 2008b), but most of the POC exported from the floodplain is then preserved in the Bengal Fan due to the sediment properties and high sedimentation rates (Galy et al., 2007). Importantly, the POC carried by the Ganges and Brahmaputra Rivers appears to include aged  $\text{POC}_{\text{biosphere}}$  eroded from the high elevations of the Tibetan Plateau (Galy and Eglinton, 2011); oxidation of this pre-aged  $\text{POC}_{\text{biosphere}}$  during river transport could represent a source of  $\text{CO}_2$  to the modern atmosphere over decadal to millennial timescales (Galy and Eglinton, 2011).

In contrast to the frontal Himalaya, the source and yield of POC eroded from the eastern margin of the Tibetan Plateau, flanked by the Longmen Shan mountains (Densmore et al., 2007) which are drained by the Yangtze River, remains poorly constrained. Like the Himalaya, this area is tectonically active and may also host pre-aged  $\text{POC}_{\text{biosphere}}$  at high elevations. But in contrast to the Himalaya and other mountainous regions where POC discharge has been quantified, the Longmen Shan has moderately low runoff ( $<1 \text{ m yr}^{-1}$ , compared to  $> 2 \text{ m yr}^{-1}$  in the areas of most prior studies reviewed by Hilton, 2017). In addition, the monsoonal climate and the

occurrence of the 2008  $M_w$  7.9 Wenchuan earthquake make this an interesting location to assess the relative roles of climate and tectonics in regulating POC erosion.

Using a pair of gauging stations on the Zagunao River (drainage area = 4486 km<sup>2</sup>), upstream and downstream of a region affected by coseismic landslides, Wang et al. (2016) showed that fluvial discharge of POC<sub>biosphere</sub> more than doubled along this reach following the Wenchuan earthquake. Here we combine the published data from Wang et al. (2016) with new suspended sediment samples from 4 additional hydrological stations which drain an area of the Longmen Shan that is much larger than that impacted by the earthquake (Li et al., 2014), covering a total drainage area of 14384 km<sup>2</sup> (Fig. 1). Samples were collected from 2005 to 2012. To constrain the compositional range of POC and its sources, we have measured a combination of [OC<sub>total</sub>],  $F_{\text{mod}}$ , and  $\delta^{13}\text{C}$  of organic carbon ( $\delta^{13}\text{C}_{\text{org}}$ ). We combine the hydrometric and geochemical data to quantify the POC discharge from the Longmen Shan. Our central aim is to quantify the fluxes of organic carbon and to establish the controls on its  $\delta^{13}\text{C}_{\text{org}}$  and  $F_{\text{mod}}$  values in rivers across this mountain range, with implications for understanding how climate regulates the erosion of carbon from the biosphere.

## 2. Materials and Methods

### 2.1 Study Area

The Min Jiang is a principal tributary of the Yangtze River and a major river draining the Longmen Shan (Fig. 1). We study three pairs of upstream (U) and downstream (D) gauging stations in the upper Min Jiang catchment: i) the Heishui River tributary (U1 = Heishui station, D1 = Shaba station); ii) the Zagunao River tributary (U2 = Zagunao, D2 = Sangping); and iii) the main stream of the Min Jiang (U3 = Zhenjianguan, D3 = Weizhou), where D3 is downstream of all stations (Fig. 1). The catchments drain the steep and high relief terrain of the Longmen Shan (Burchfiel et al., 1995; Densmore et al., 2007) with drainage areas ranging from 1720 km<sup>2</sup> at station U1 to 18870 km<sup>2</sup> at station D3 (Table 1). This region has a long, complex deformation history resulting from collision of the Songpan–Ganze terrain with the Yangtze block (Burchfiel et al., 1995) which developed in the Mesozoic time (Burchfiel et al., 1995; Chen and Wilson, 1996) and was reactivated in the Cenozoic (Burchfiel et al., 1995), as recently manifested by the 2008  $M_w$  7.9 Wenchuan

earthquake (Burchfiel et al., 2008). The plateau margin comprises Proterozoic granitoids and high-grade metamorphic rocks, including Neoproterozoic crystalline massifs, overlain by a Paleozoic passive margin sequence and Mesozoic foreland basin sediments (Fig. 1b). Our study reaches are underlain by metamorphosed Triassic Songpan-Ganze flysch-type sediments intruded by granitic plutons. Thus, a striking feature of the Min Jiang drainage area is the wide range of lithologies subject to spatially heterogeneous erosion in the Longmen Shan (Liu-Zeng et al., 2011).

The regional climate is influenced by the East Asian and Indian summer monsoons, which lead to a rainy season from May to October that supplies 70% – 80% of the annual precipitation. The upper Min Jiang catchment is characterized by an alpine climate, with mean annual temperature below 13 °C (Zhang et al., 2005; Zhang, 2008). The dominant landscape types are forest, shrubland and grassland, which are very similar in terms of areal coverage (each comprising ~30% of the land area in the Min Jiang; Fig. 1c; Editorial Committee for Vegetation of China, Chinese Academy of Sciences, 2007). With the exception of the upstream catchment above the Zagunao station (station U2), the original forests were harvested mainly from the 1950s to the 1970s and replanted since the 1990s (Cui et al., 2012). Due to the high relief, steep topography and precipitation gradient, both the forest and soil types vary with altitude. Shrub is dominant in the arid river valleys from 1300 m to 2600 m (Zhang, 2008). The soils are dominated by Hapli-Udic Cambosols and Hapli-Ustic Cambosols and mostly developed on alluvium and colluvial accumulations. Forest appears from 1800 m to 3900 m, with underlying Mollic- or Umbri-Gelic Cambosols that are deeper and are rich in organic carbon (Xian et al., 2009). At higher elevations are shrubland and alpine meadow, characterized by Matti-Gelic Cambosols (Zhang, 2008). Soil organic carbon stocks range from  $9 \times 10^3$  tC km<sup>-2</sup> to  $22 \times 10^3$  tC km<sup>-2</sup> and vary with forest type and elevation (Xian et al., 2009).

The tectonic setting, topography, and climate combine to set temporal and spatial patterns in erosion. The decadal basin-averaged erosion rate calculated from sediment fluxes measured at 62 hydrological gauging stations is  $\sim 0.5$  mm yr<sup>-1</sup> along the eastern margin of the plateau and decreases towards the Tibetan Plateau, to 0.05 mm yr<sup>-1</sup> (Liu-Zeng et al., 2011). This result is generally comparable to erosion rates over millennial timescales derived from cosmogenic <sup>10</sup>Be measurements (Ouimet et al., 2009; Godard et al., 2010) and Myr-scale erosion rates inferred from

thermochronology (Ouimet, 2010). Erosion rates of our studied catchments are moderate, ranging from 0.1 to 0.2 mm yr<sup>-1</sup> (Liu-Zeng et al., 2011). Mean annual precipitation has no clear impact on the spatial patterns of erosion rate (Liu-Zeng et al., 2011), but intense runoff events play an important role in evacuating sediment in river suspended loads (Wang et al., 2015). Over thousands of years, earthquakes and associated landslides are thought to be a major contributor of sediment and a main driver of the sediment fluxes and long-term denudation rates (Li et al., 2017).

## 2.2 The Wenchuan Earthquake

The M<sub>w</sub> 7.9 Wenchuan earthquake on 12 May 2008 ruptured the Yingxiu-Beichuan and Pengguan faults that bound the mountain front. The earthquake triggered tens of thousands of landslides (Parker et al., 2011; Li et al., 2014) which increased suspended sediment fluxes in the years that followed (Wang et al., 2015) and also increased POC discharge in rivers impacted by landslides (Wang et al., 2016). Most of the study area here did not experience significant earthquake-triggered landslides based on landslide mapping by Li et al. (2014). Stations U1, D1 and U3 were >50 km from the fault rupture (Fig. 1a), and the proportion of their catchment areas with mapped landslides was <0.01%. Previous work has established that there were no significant changes in suspended sediment fluxes following the earthquake at these gauging stations (Wang et al., 2015), consistent with the lack of observed landslides.

The catchments of three of the gauging stations studied here experienced moderate numbers of earthquake-triggered landslides: two stations on the Zagunao River (station U2 and D2), which were the focus of investigation by Wang et al. (2016), and the middle reaches of the Min Jiang (D3). With moderate landslide impact (~0.3% of the downstream area), the ratio between POC<sub>biosphere</sub> discharge (tC yr<sup>-1</sup>) at U2 and D2 (the “downstream POC<sub>biosphere</sub> gain”) doubled in the four years after the earthquake (Wang et al., 2016). Our sample stations do not capture the locations with the highest amount of coseismic landslides per unit area (Li et al., 2014). For these reasons, we do not focus on the impact of the 2008 Wenchuan earthquake in our analysis here, instead noting that published work develops interpretations about the earthquake effects as far as currently available data allow (Wang et al., 2016).

## 2.3 River Sampling

The Chinese Bureau of Hydrology (CBH) maintains the gauging stations used in this study from the upper Min Jiang; water discharge ( $Q_w$ ,  $m^3 s^{-1}$ ) is measured daily and suspended sediment samples are collected and archived at these stations (Fig. 1). The CBH collected suspended sediment samples up to 8 times per day during April to October from 2005 to 2009 by filtering 2 or 4 L of water through  $\sim 1 \mu m$  paper filters (Ministry of Water Resources of China, 2007). The water was collected with a depth-integrated sampler (Ministry of Water Resources of China, 2007; Wang et al., 2015). In addition, suspended sediment samples from 2009 to 2012 were collected weekly for geochemical analysis by CBH staff from stations U1, D2, U3 and D3. For those samples, 1 L of water was collected and passed through a  $0.7 \mu m$  GF/F filter which was then dried at  $60^\circ C$  and stored in a petri dish (Wang et al., 2016).

The suspended load samples were collected over a wide range of hydrological conditions, as illustrated by the range of suspended sediment concentrations (SSC,  $g L^{-1}$ ) sampled at each gauging station (Electronic Annex Table EA1). These ranged from:  $0.01 g L^{-1}$  to  $14.33 g L^{-1}$  at station U1;  $0.03 g L^{-1}$  to  $12.11 g L^{-1}$  at station D1;  $0.08 g L^{-1}$  to  $25.56 g L^{-1}$  at station U2;  $0.03 g L^{-1}$  to  $12.87 g L^{-1}$  at station D2;  $0.04 g L^{-1}$  to  $38.83 g L^{-1}$  at station U3; and  $0.02 g L^{-1}$  to  $8.09 g L^{-1}$  at station D3.

To help constrain the composition of POC sources in the landscape, samples of river bed material, bedrock, vegetation and soil were sampled from the study area in 2014 (Fig. 1). River bed materials ( $n = 37$ ) were collected at the surface of the river bed during low water level. Approximately 1 kg of sand- to mud-sized material was collected and stored in clean sealed bags. Near these sites, bedrock samples were collected ( $n = 20$ ), with weathered surfaces removed prior to collection. Wood and twig fragments were sampled from bars on rivers ( $n = 54$ ) and are likely to represent material eroded and transported during the previous rainy season. At 9 locations, soil materials were collected from O to C horizons with a trowel and transferred to sealed bags ( $n = 22$ ). After returning to the laboratory, all samples were dried at  $60^\circ C$  in the oven and stored in sealed bags.

## 2.4 Analytical Methods

Suspended load samples were removed from the filters using gentle agitation with a spatula and were homogenized using a mortar and pestle. The bedrock, soil and bed material samples were ground to a powder by a vibratory disc mill. The vegetation

samples were cleaned of surface decomposed material and were ground in a cryogenic grinding machine. All samples apart from the vegetation were subject to a carbonate removal protocol using a liquid 4M HCl leach at 80°C for 4 hours (see details in Clark et al., 2013; Wang et al., 2016). This is known to remove a labile component of the organic matter (Galy et al., 2007) and so here our results reflect acid insoluble organic carbon.

The  $[OC_{total}]$  was determined by combustion at 1020°C in  $O_2$  within a Costech CHN elemental analyzer (EA).  $\delta^{13}C_{org}$  was determined by continuous flow from the EA coupled via CONFLO-III to a Thermo-Delta-V isotope ratio mass spectrometer (Hilton et al., 2008b; Clark et al., 2013) in the Stable Isotope Biogeochemistry Laboratory at Durham University. Values were normalized based on measured values of several standards and reported in  $\delta^{13}C$  notation relative to Vienna Pee Dee Belemnite (VPDB). Duplicates of the samples ( $n = 42$ ) returned an average standard deviation on  $\delta^{13}C$  of  $\pm 0.1\%$  and an average relative standard deviation on  $[OC_{total}]$  values of  $\pm 2.5\%$ , and we take these as the average precision of the analyses and report it as  $\pm 1$  standard deviation. Radiocarbon ( $^{14}C$ ) activity of samples was measured by accelerator mass spectrometry (AMS) after carbonate removal and graphitization at the Keck-Carbon Cycle AMS Facility at the University of California, Irvine, USA, and is reported as fraction modern ( $F_{mod}$ ).

The suspended load samples from 2005 – 2009 were collected on paper filters, and we quantified the filter blank to correct the contribution of C from the paper to the samples. The detailed methods of the blank correction on  $[OC_{total}]$ ,  $\delta^{13}C$  and  $F_{mod}$  values are found in Wang et al. (2016). In summary, the filter blank contributed  $<10\%$  of the mass of carbon in 98% of the samples analysed.  $[OC_{total}]$  was corrected as a linear function of sample mass, and  $\delta^{13}C$  and  $F_{mod}$  values were corrected by the paper contribution and  $\delta^{13}C$  and  $F_{mod}$  of blank samples (combusted quartz sand; Wang et al., 2016).

## 2.5 Quantification of $POC_{biosphere}$ and $POC_{petro}$ Contributions

Different approaches have been used to trace the sources of POC and quantify their contributions to river suspended loads. Radiocarbon activity has proven to be one of the most robust ways to constrain POC sources because of the difference between  $POC_{petro}$  (which will have no measurable  $^{14}C$  above analytical background for sample

ages of >60 ka) and  $\text{POC}_{\text{biosphere}}$  which contains  $^{14}\text{C}$  derived from atmospheric  $\text{CO}_2$  during recent photosynthesis (Blair et al., 2003; Komada et al., 2004; Galy et al., 2007; Hilton et al., 2008b). Other bulk geochemical analyses, such as elemental (e.g., C/N) and stable C isotopic ratios, can also be used to constrain the source of  $\text{POC}_{\text{biosphere}}$ , and can provide complementary evidence for aged  $\text{POC}_{\text{biosphere}}$  (Hilton et al., 2015; Clark et al., 2017).

Using the measured  $F_{\text{mod}}$  and  $[\text{OC}_{\text{total}}]$  of river sediments, Galy et al. (2008a) applied a binary mixing model (after Blair et al., 2003) to describe the mixing of  $\text{POC}_{\text{biosphere}}$  and  $\text{POC}_{\text{petro}}$  in river sediments, expressed as:

$$F_{\text{mod}} \times [\text{OC}_{\text{total}}] = F_{\text{mod-bio}} \times [\text{OC}_{\text{biosphere}}] + F_{\text{mod-petro}} \times [\text{OC}_{\text{petro}}] \quad (1)$$

where  $F_{\text{mod}}$ ,  $F_{\text{mod-bio}}$ , and  $F_{\text{mod-petro}}$  are the radiocarbon compositions of the total, biospheric, and petrogenic POC, respectively; and  $[\text{OC}_{\text{total}}]$ ,  $[\text{OC}_{\text{biosphere}}]$ , and  $[\text{OC}_{\text{petro}}]$  are the contents of  $\text{POC}_{\text{total}}$ ,  $\text{POC}_{\text{biosphere}}$ , and  $\text{POC}_{\text{petro}}$  expressed as % of dry weight. If the sediment mixture is well homogenised, then  $[\text{OC}_{\text{petro}}]$  of the total sediment can be written as:

$$[\text{OC}_{\text{petro}}] = [\text{OC}_{\text{total}}] - [\text{OC}_{\text{biosphere}}] \quad (2)$$

Because the rock-derived POC is radiocarbon-dead, we can substitute  $F_{\text{mod-petro}} = 0$  into equations (1):

$$F_{\text{mod}} = \frac{F_{\text{mod-bio}} \times [\text{OC}_{\text{total}}] - F_{\text{mod-bio}} \times [\text{OC}_{\text{petro}}]}{[\text{OC}_{\text{total}}]} \quad (3)$$

$F_{\text{mod}}$  of the samples is a hyperbolic function of  $[\text{OC}_{\text{total}}]$  with curvature that is defined by  $[\text{OC}_{\text{petro}}]$  (Hemingway et al., 2018). We fit the data from each station and solve equation (3) for  $F_{\text{mod-bio}}$  and  $[\text{OC}_{\text{petro}}]$  using non-weighted orthogonal distance regression in the software of OriginPro 2017.

In addition,  $\text{POC}_{\text{petro}}$  often has a distinct  $\delta^{13}\text{C}_{\text{org}}$  and carbon content when compared to  $\text{POC}_{\text{biosphere}}$  (e.g., Hilton et al., 2010). These bulk measurements can be combined to investigate the nature of POC source and quantify the  $\text{POC}_{\text{petro}}$  and  $\text{POC}_{\text{biosphere}}$  contributions.

## 2.6 Quantification of POC Discharge

The CBH dataset includes daily, flow-weighted mean SSC measurements, which can be combined with daily mean  $Q_w$  to accurately quantify mean daily suspended sediment discharge ( $Q_{ss}$ ,  $g\ s^{-1}$ ). These daily data can be summed to quantify annual suspended sediment discharge (Wang et al., 2015). The suspended sediment sample archive is very large, and it was only possible to measure  $[OC_{total}]$  on a subset of samples from each river basin. As a result, POC concentrations ( $[POC_{total}]$ ,  $g\ C\ m^{-3}$ ) have a lower temporal resolution compared to SSC. Therefore, to estimate POC discharge ( $Q_{POC}$ ,  $g\ s^{-1}$ ) we examine the linear relationship between log-transformed SSC and  $[POC_{total}]$  (Fig. 2) for each station and apply this empirical model to the daily  $Q_w$  data.

To quantify petrogenic and biospheric POC discharge ( $Q_{POC-petro}$  and  $Q_{POC-bio}$ ) we used the outputs of the mixing analyses which quantify  $[OC_{petro}]$  for each sub-basin. Following the hyperbolic regression,  $Q_{POC-petro}$  was calculated by multiplying  $Q_{ss}$  by  $[OC_{petro}]$ . The difference between  $Q_{POC}$  and  $Q_{POC-petro}$  is the biospheric POC discharge ( $Q_{POC-bio}$ ). Errors were propagated from the uncertainties on  $[OC_{total}]$  blank correction,  $Q_{ss}$ ,  $[OC_{petro}]$ , and the relationship between SSC and  $[POC_{total}]$  (Wang et al., 2015). Because SSC measurements are not available at station D3 (Weizhou) and gauging station D2 (Sangping) was not in operation in 2012, we calculate the  $Q_{ss}$  and  $Q_{POC}$  from 2006 to 2011 for D2 and from 2006 to 2012 for U1, D1, U2, and U3.

### 3. Results

The six study sub-catchments have contrasting bedrock geology, elevation ranges and vegetation distributions (Fig. 1). Therefore, while plotting the data together can illustrate broad patterns across the Longmen Shan mountains (e.g. Fig. 3), it is more insightful to examine the catchments individually. Despite the differences between catchments, we observe common contrasts between river suspended sediments and bed materials for each catchment in several respects (which are expanded on in the sections which follow): (1) suspended sediments at all sites have higher  $[OC_{total}]$  than their corresponding bed materials, (2) all bed materials are enriched in  $^{13}C$  compared to suspended sediments (Fig. 3), and (3) where  $^{14}C$  measurements are available, the  $F_{mod}$  values are much lower in river bed materials than in suspended sediments. These broad patterns match observations made in other mountain rivers draining

sedimentary bedrock (Blair et al., 2003; Leithold et al., 2006; Galy et al., 2008b; Hilton et al., 2010, 2017; Clark et al., 2013) and are consistent with aforementioned mixing of biospheric and petrogenic components if the latter are concentrated in the bed sediments.

Herein the catchments are paired into upstream (U) and downstream (D) sites and the isotopic composition of river POC is discussed in more detail. All the individual suspended load sample data are provided in Table EA1 with summaries in Table EA2.

### 3.1 POC in the Heishui River (Stations U1 and D1)

Two gauging stations are located along the Heishui River tributary: Heishui station (U1) upstream and Shaba station (D1) downstream (Fig. 1). The mean  $[\text{OC}_{\text{total}}]$  of suspended sediment from station U1 is  $0.99 \pm 0.30\%$  ( $\pm 1\sigma$ ,  $n = 41$ ) and from station D1 is  $1.13 \pm 0.71\%$  ( $n = 36$ ). The  $\delta^{13}\text{C}_{\text{org}}$  of POC has a mean of  $-25.4 \pm 0.7\text{‰}$  for station U1 and a mean of  $-25.0 \pm 0.9\text{‰}$  for station D1. The bulk  $\delta^{13}\text{C}_{\text{org}}$  for station U1 and D1 is positively correlated with  $1/[\text{OC}_{\text{total}}]$  ( $r^2 = 0.34$  and  $0.79$ ,  $p < 0.01$ ; Fig. 3). This relationship is similar to trends observed in other mountain river catchments (Hilton et al., 2008b; 2010) and may indicate a mixing control on the  $\delta^{13}\text{C}_{\text{org}}$  values. The  $F_{\text{mod}}$  of the suspended sediment ranges from  $0.59 \pm 0.005$  to  $0.79 \pm 0.006$  ( $n = 6$ ) at U1 and from  $0.45 \pm 0.005$  to  $1.02 \pm 0.006$  ( $n = 5$ ) at D1. The measured  $F_{\text{mod}}$  negatively correlates with both  $\delta^{13}\text{C}_{\text{org}}$  ( $r^2 = 0.75$ ,  $p = 0.06$ ; Fig. 4), and  $1/[\text{OC}_{\text{total}}]$  ( $r^2 = 0.95$ ,  $p < 0.01$ ; Fig. 4) for station D1 but not for station U1.

The  $[\text{OC}_{\text{total}}]$  of the bed materials is  $0.21 \pm 0.03\%$  ( $n = 5$ ) and  $0.30 \pm 0.07\%$  ( $n = 10$ ) for stations U1 and D1, respectively. The mean  $\delta^{13}\text{C}_{\text{org}}$  of bed material is  $-21.5 \pm 3.2\text{‰}$  to  $-20.4 \pm 1.6\text{‰}$  in the upstream and downstream, respectively.

### 3.2 POC in the Zagunao River (Stations U2 and D2)

Suspended sediments were collected from 2005 to 2009 at station U2 and from 2005 to 2011 at station D2, located at the upstream and downstream ends of the study reach on the Zagunao River, respectively. The data from these two stations were used by Wang et al. (2016) to assess the impact of the 2008 Wenchuan earthquake on  $\text{POC}_{\text{biosphere}}$  erosion. Summarized here for completeness, the  $[\text{OC}_{\text{total}}]$  of the suspended sediment is similar at both stations with means of  $0.96 \pm 0.27\%$  ( $n = 40$ )

at U2 and  $0.96 \pm 0.45\%$  ( $n = 114$ ) at D2. The mean  $\delta^{13}\text{C}_{\text{org}}$  of POC is  $-22.2 \pm 1.7\%$  at U2 and  $-23.7 \pm 1.1\%$  at D2. The  $\delta^{13}\text{C}_{\text{org}}$  significantly correlates with  $1/[\text{OC}_{\text{total}}]$  for both stations ( $r^2 = 0.23$  and  $0.27$  for stations U2 and D2,  $p < 0.01$ ; Fig. 4).  $F_{\text{mod}}$  of the POC from station U2 ranges from  $0.27 \pm 0.006$  to  $0.74 \pm 0.005$  ( $n = 9$ ) and at station D2 ranges from  $0.46 \pm 0.001$  to  $0.94 \pm 0.006$  ( $n = 16$ ).  $F_{\text{mod}}$  is linearly correlated with  $\delta^{13}\text{C}_{\text{org}}$  and  $1/[\text{OC}_{\text{total}}]$  in both stations ( $r^2 = 0.45\text{--}0.67$ ,  $p < 0.05$ ; Fig. 4).

The mean  $[\text{OC}_{\text{total}}]$  of the river bed materials is  $0.45 \pm 0.09\%$  ( $n = 5$ ) at station U2 and is  $0.32 \pm 0.09\%$  ( $n = 7$ ) at station D2. The  $\delta^{13}\text{C}_{\text{org}}$  values of river bed materials in the Zagunao River are the most variable across the sample set, ranging from  $-19.8 \pm 0.1\%$  to  $-13.2 \pm 0.1\%$  at station U2 and from  $-19.9 \pm 0.1\%$  to  $-15.4 \pm 0.1\%$  at station D2. They are also the most  $^{13}\text{C}$ -enriched, with mean  $\delta^{13}\text{C}_{\text{org}}$  values =  $-15.6 \pm 2.7\%$  for U2 and  $-18.3 \pm 1.6\%$  for D2. Each station has one radiocarbon analysis for the bed material. A very low radiocarbon activity was observed in both samples ( $F_{\text{mod}} = 0.02$  and  $0.06$ ; Table EA3), consistent with the river bed material being dominated by  $\text{POC}_{\text{petro}}$ .

### 3.3 POC in the Min Jiang (Stations U3 and D3)

The Zhenjianguan (U3) station is located in the upstream part of the Min Jiang catchment, while the Weizhou station (D3) is the most-downstream station after the junction of the Heishui and Zagunao tributaries (Fig. 1). The  $[\text{OC}_{\text{total}}]$  of suspended sediment has a mean of  $1.09 \pm 0.41\%$  ( $n = 54$ ) at station U3 and a mean of  $0.62 \pm 0.27\%$  ( $n = 35$ ) at station D3. The mean  $\delta^{13}\text{C}_{\text{org}}$  of POC is  $-25.5 \pm 0.8\%$  at station U3 and  $-24.5 \pm 1.1\%$  at station D3. The bulk  $\delta^{13}\text{C}_{\text{org}}$  is weakly but significantly positively correlated with  $1/[\text{OC}_{\text{total}}]$  ( $r^2 = 0.16$  and  $0.15$ ,  $p < 0.05$ ; Fig. 3). The  $F_{\text{mod}}$  of the suspended sediment at station U3 ranges from  $0.59 \pm 0.005$  to  $0.87 \pm 0.006$  ( $n = 8$ ) and negatively correlates with  $\delta^{13}\text{C}_{\text{org}}$  ( $r^2 = 0.53$ ,  $p < 0.05$ ; Fig. 4).  $F_{\text{mod}}$  of the POC at D3 has a similar range from  $0.58 \pm 0.001$  to  $0.86 \pm 0.002$  ( $n = 5$ ), which is linearly related to  $\delta^{13}\text{C}_{\text{org}}$  and  $1/[\text{OC}_{\text{total}}]$  ( $r^2 = 0.96$  and  $0.84$ ,  $p < 0.05$ ; Fig. 4).

Three river bed material samples upstream of U3 have mean  $[\text{OC}_{\text{total}}]$  values  $0.20 \pm 0.03\%$ , lower than those of the suspended sediment. The  $\delta^{13}\text{C}_{\text{org}}$  values of these bed materials average to  $-21.8 \pm 1.6\%$ . River bed materials collected along the main stem between stations U3 and D3 ( $n = 7$ ) have a mean  $[\text{OC}_{\text{total}}]$  of  $0.24 \pm 0.12\%$  and a mean  $\delta^{13}\text{C}_{\text{org}}$  is  $-22.3 \pm 2.7\%$ .

### 3.4 Bedrock

Twenty bedrock samples were collected throughout the upper Min Jiang catchment, covering a wide range of lithologies including phyllite, schist, shale, slate, mudstone, and granite (Table EA3). The  $[OC_{total}]$  of bedrock samples from the upper Min Jiang is low with a mean of  $0.24 \pm 0.30\%$  but displays considerable variation between  $<0.01\%$  and  $0.94\%$ . The  $\delta^{13}C_{org}$  of these bedrock samples has a mean of  $-20.8 \pm 6.4\%$ , and also has a large range (Electronic Annex Fig. EA1). These values are more similar to the river bed materials than to the suspended sediments, but do cover some of the range of values measured in the suspended sediments. Very high  $\delta^{13}C_{org}$  values ( $>-15\%$ ) of bedrock are found in each sub-basin. The HCl leach protocol used here is towards the higher end of molarities of acid used by previous studies (Komada et al., 2004; Galy et al., 2007), so it is difficult to invoke residual carbonate as a factor influencing  $\delta^{13}C_{org}$  values.

River bed materials are often considered as a mixture of bedrock from within each catchment with relatively minor biospheric carbon input (Hilton et al., 2010; Clark et al., 2017). In our study, the OC content and isotopic composition of the river bed materials fall within the range defined by bedrock samples and could be explained as the mixture of different types of rocks.

### 3.5 Vegetation and Soil

The  $[OC_{total}]$  of wood and twig fragments is much higher than for other types of samples, with values ranging from  $40.04 \pm 1.00\%$  to  $52.05 \pm 1.30\%$  and a mean of  $44.71 \pm 1.98\%$  ( $n = 54$ ).  $\delta^{13}C_{org}$  for these samples averages  $-26.1 \pm 1.8\%$  and has a range from  $-30.4 \pm 0.1\%$  to  $-22.6 \pm 0.1\%$ . These values indicate no C4 plants in our samples according to the global survey of plant carbon isotope compositions (Körner et al., 1988), consistent with our expectations for this region.

Soils were collected from different horizons. The O horizons are richer in organic carbon with a mean  $[OC_{total}]$  of  $6.51 \pm 1.64\%$  ( $n = 3$ ) ranging from  $4.91 \pm 0.12\%$  to  $8.20 \pm 0.20\%$ . The OC in these horizons is depleted in  $^{13}C$  with mean  $\delta^{13}C_{org}$  at  $-28.5 \pm 0.9\%$  ranging from  $-29.4 \pm 0.1\%$  to  $-27.6 \pm 0.1\%$ . Horizon A reaches  $\sim 50$  cm in depth at the sites we sampled. The  $[OC_{total}]$  and  $\delta^{13}C_{org}$  of horizon A both vary between different sites. The  $[OC_{total}]$  ranges from  $0.67 \pm 0.02\%$  to  $4.09 \pm 0.10\%$  with a mean of  $1.87 \pm 1.11\%$  ( $n = 10$ ), and associated  $\delta^{13}C_{org}$  ranges from  $-28.0 \pm 0.1\%$  to

-24.3 ± 0.1‰ with a mean of -26.3 ± 1.0‰. Horizons B to C range in thickness from 3 cm to over 1 m at our sampled sites. Because some rock detritus was mixed in these layers, [OC<sub>total</sub>] is low at 0.38 ± 0.25% ranging from 0.14 ± 0.00% to 0.91 ± 0.02% and the δ<sup>13</sup>C<sub>org</sub> is -22.7 ± 2.4‰ ranging from -25.5 ± 0.1‰ to -18.0 ± 0.1‰ (n = 9). The δ<sup>13</sup>C<sub>org</sub> of all the soil samples is positively correlated with 1/[OC<sub>total</sub>] ( $r^2 = 0.42$ ,  $p < 0.01$ ).

## 4. Discussion

### 4.1 Petrogenic Organic Carbon Influences the δ<sup>13</sup>C<sub>org</sub> of Riverine POC

The δ<sup>13</sup>C<sub>org</sub> values of fine grained fluvial-sourced sedimentary deposits can be an important archive from which to interrogate the operation of the carbon cycle in the geological past (e.g. Xu et al., 2017). However, in mountain river catchments erosion of rocks can add POC<sub>petro</sub> and this recycled component has been shown to strongly influence the δ<sup>13</sup>C<sub>org</sub> values of river POC in Taiwan (Hilton et al., 2010), the Himalaya (Galy et al., 2008b) and the Peruvian Andes (Clark et al., 2013). The Longmen Shan is a major source of sediment to the Sichuan Basin, and here we examine the role that petrogenic carbon might play in controlling the δ<sup>13</sup>C<sub>org</sub> values of river POC.

The δ<sup>13</sup>C<sub>org</sub> values are linearly correlated with 1/[OC<sub>total</sub>] in the suspended samples collected at each station (Fig. 3). In addition, the most <sup>14</sup>C-depleted suspended load samples generally have the highest δ<sup>13</sup>C<sub>org</sub> values (Fig. 4). These patterns are consistent with observations from other studies of mountain rivers (Hilton et al., 2010; Marwick et al., 2015). The relationship can be explained by a mixing of POC<sub>petro</sub> from rocks, which here is low in [OC<sub>total</sub>], <sup>13</sup>C enriched and <sup>14</sup>C depleted, with POC<sub>biosphere</sub> from the vegetation and surface soils, which is high in [OC<sub>total</sub>], generally <sup>13</sup>C depleted and <sup>14</sup>C enriched (Leithold et al., 2006; Hilton et al., 2015; Clark et al., 2017). This mixing is also suggested by the linear relationships of  $F_{mod}$  with δ<sup>13</sup>C<sub>org</sub> and with 1/[OC<sub>total</sub>] of the suspended sediment samples (Fig. 4). Because of the high turbidity of these mountain rivers, especially at times of high runoff (Wang et al., 2015), the *in situ* production of planktonic and bacterial carbon is likely to be a minor component of POC<sub>biosphere</sub>.

Four suspended load POC samples from station U2 have δ<sup>13</sup>C<sub>org</sub> values >-20‰, which are higher than the most enriched values reported from other mountain rivers where C3 plants dominate (Marwick et al., 2015). The river bed materials are

dominated by  $\text{POC}_{\text{petro}}$  and could represent an averaged composition of  $\text{POC}_{\text{petro}}$  due to the mixing of rock clasts during sediment transport (Hilton et al., 2010; Wang et al., 2016; Clark et al., 2017). The measured  $\delta^{13}\text{C}_{\text{org}}$  of the river bed material collected within the same catchment is  $-15.6 \pm 2.7\text{‰}$ , consistent with the  $^{13}\text{C}$ -enriched  $\text{POC}_{\text{petro}}$ . Isotopically enriched organic matter was found in bed material samples from other stations, with values that fall within the range of the  $\delta^{13}\text{C}_{\text{org}}$  values of the bedrock (Table EA3). High  $\delta^{13}\text{C}_{\text{org}}$  values have been reported in landslide sediments and bed materials from another study in this area (Hara, 2016). The low  $F_{\text{mod}}$  also support the importance of  $^{14}\text{C}$ -depleted  $\text{POC}_{\text{petro}}$  as the source of higher  $\delta^{13}\text{C}_{\text{org}}$  values in the suspended load (Fig. 4).

The high  $\delta^{13}\text{C}_{\text{org}}$  values of the organic matter in bedrocks of the Longmen Shan may reflect metamorphic reactions during the complicated tectonic history of this region (Robert et al., 2010). Metamorphic processes can enrich the isotope ratio of organic matter by devolatilization of isotopically light methane in equilibrium with graphite (Hoefs and Frey, 1976; Schwab et al., 2005). Therefore, high grade metamorphic rocks can have high  $\delta^{13}\text{C}_{\text{org}}$  values (Andreae, 1974), regardless of the terrestrial or marine origin of the organic matter, or their geological age (Hayes et al., 1999). In our study, some very high  $\delta^{13}\text{C}_{\text{org}}$  values are found in samples from high grade metamorphic terrains.

The high  $\delta^{13}\text{C}_{\text{org}}$  values of bedrocks in the Longmen Shan give perhaps the most extreme example to date of how  $\text{POC}_{\text{petro}}$  can impact the stable carbon isotope composition of POC carried by mountain rivers (Komada et al., 2004; Hilton et al., 2010; Marwick et al., 2015; Clark et al., 2017). If this  $\text{POC}_{\text{petro}}$  persists downstream and contributes to sedimentary deposits upon exiting the mountain belt, it may influence the bulk  $\delta^{13}\text{C}_{\text{org}}$  of detrital material (Hilton et al., 2010; Kao et al., 2014). These shifts could be incorrectly assigned to changes expected from C4 organic matter inputs, or may potentially complicate the interpretation of the stable isotopic composition in the Sichuan Basin in terms of carbon cycle processes (Xu et al., 2017), particularly where  $[\text{OC}_{\text{total}}]$  are  $< 1\%$  and  $\text{POC}_{\text{petro}}$  may contribute significantly to the mass of bulk organic carbon.

## 4.2 Evidence for Aged Biospheric POC

Aged biospheric POC has been identified in the major frontal Himalayan tributaries that drain high altitudes of the Tibetan Plateau (Galy and Eglinton, 2011). Here we examine evidence for this component in rivers draining the Longmen Shan. The isotopic and elemental compositions of POC in the upper Min Jiang suggest that the POC is a mixture of  $\text{POC}_{\text{biosphere}}$  and  $\text{POC}_{\text{petro}}$ . However, these patterns do not preclude mixing of  $\text{POC}_{\text{biosphere}}$  from young OC in vegetation and surface soil with aged OC from deeper soils (Fig. 3): the  $\delta^{13}\text{C}_{\text{org}}$  values of soil horizons A and B-C generally fall on the mixing line between C3 plants (and O-horizon soil) and river bed material (Fig. 3), such that the younger and older sources of  $\text{POC}_{\text{biosphere}}$  cannot be separated based on  $\delta^{13}\text{C}_{\text{org}}$  values alone. To explore the age structure of the POC in these rivers in more detail, we turn to a binary mixing model based on hyperbolic regression using  $F_{\text{mod}}$  and  $[\text{OC}_{\text{total}}]$  (Equation 3; Hemingway et al., 2018).

We include the bed material samples for the regression at each station. However, only two samples at stations U2 and D2 have been analyzed for radiocarbon activity, with  $F_{\text{mod}} = 0.02$  and  $0.06$ , respectively. The bed materials of all stations appear distinct from vegetation and soil O and A layer measurements in terms of their stable isotopic composition, and are more similar to the bedrock samples (Fig. EA1), suggesting a dominance of  $\text{POC}_{\text{petro}}$  (Fig. 3). Therefore, we assume that the measured  $^{14}\text{C}$  activity of bed materials from U2 and D2 are representative of the petrogenic component for U1, D1, U3 and D3, and assume their  $F_{\text{mod}} = 0.04 \pm 0.02$  (Fig. 5). A range of continuous  $[\text{OC}_{\text{petro}}]$  and  $F_{\text{mod-bio}}$  were used to generate a contour of Root Mean Square Error (RMSE) of the orthogonal distance regression, giving us a clear pattern of the predicted  $[\text{OC}_{\text{petro}}]$  and  $F_{\text{mod-bio}}$  values for each station and the reliability of the regression (Fig. EA2). For stations D1, U3 and D3, the regression through the data was fitted both with and without the assumed river bed material  $F_{\text{mod}}$  value, and returned the same predicted  $[\text{OC}_{\text{petro}}]$  and  $F_{\text{mod-bio}}$  values within uncertainty. This suggests the assumed low  $F_{\text{mod}}$  values for the river bed materials is valid.

The hyperbolic binary mixing model returns an average  $F_{\text{mod-bio}}$  which ranges from lower values of  $0.82 \pm 0.09$  ( $\pm$  standard error, SE) at U1 and  $0.84 \pm 0.08$  at U3 to  $1.06 \pm 0.05$  at D1 (Table 1; Fig. 5). These correspond to  $^{14}\text{C}$  ages from  $\sim 1620 +980/-870$   $^{14}\text{C}$  years to 'modern'. The estimated  $[\text{OC}_{\text{petro}}]$  ranges from  $0.13 \pm 0.10\%$  to  $0.36 \pm 0.11\%$ . These  $[\text{OC}_{\text{petro}}]$  values are consistent with the range of measured  $[\text{OC}_{\text{total}}]$

of bedrocks (Fig. EA1), which supports the use of bed materials as a  $\text{POC}_{\text{petro}}$  end member (Hilton et al., 2010) and the assumption that they have very low  $F_{\text{mod}}$ .

Within  $\pm 1\text{SE}$  confidence intervals, the biospheric OC ages are oldest at two upstream stations which drain the high elevations of the eastern Tibetan Plateau, with  $^{14}\text{C}$  ages of biospheric OC of  $1620 \pm 980/-870$  and  $1420 \pm 750/-690$   $^{14}\text{C}$  years old at stations U1 and U3, respectively. The ages of the bulk biospheric POC in our study area are much younger than those determined for large Arctic rivers which drain extensive peat soils (Feng et al., 2013; Hilton et al., 2015) but are comparable to headwaters of the Amazon River (Bouchez et al., 2010; Clark et al., 2017). Studies from other rivers draining the Tibetan Plateau also showed thousand-year-old OC in the Ganges-Brahmaputra system (Galy and Eglinton, 2011) and values of over 3000  $^{14}\text{C}$  year in the Yellow River (Tao et al., 2015). While uncertainties remain because of the size of our sample sets (Fig. 5) and the limited number of  $^{14}\text{C}$  analysis for bed materials, our new data suggest that aged  $\text{POC}_{\text{biosphere}}$  could be a widespread feature of the high elevations of the Tibetan Plateau.

The comparison of biospheric carbon age, concentration, and loading between upstream and downstream locations is important for understanding the processing of river POC (Bouchez et al., 2010). The mean biospheric OC ages are different at the  $\pm 1\text{SE}$  confidence level between upstream and downstream sites, with  $F_{\text{mod-bio}} = 0.82 \pm 0.09$  at U1, and  $F_{\text{mod-bio}} = 1.06 \pm 0.05$  at D1, while  $F_{\text{mod-bio}} = 0.84 \pm 0.08$  at station U3 contrasts with  $F_{\text{mod-bio}} = 1.04 \pm 0.06$  at D3 (Fig. 5). These differences could reflect degradation of some components of aged biospheric carbon, representing an emission of  $\text{CO}_2$  to the atmosphere from a carbon reservoir of millennial age (Galy and Eglinton, 2011). It also could result from the transformation of aged particulate phases to the dissolved OC pools. The observed differences in age from upstream to downstream could also reflect addition of younger OC mixing during transit downstream. However, the differences are not significant at the 95% confidence level, leaving open questions about how much change is in fact taking place along these rivers. In part, this uncertainty is inherent in the mixing approach adopted here. Future work could shed more light on downstream changes by analyzing the abundance and isotope composition of biomarkers (e.g. Galy and Eglinton, 2011; Ponton et al., 2014), and/or the  $^{14}\text{C}$  activity of distinct pools of organic matter, for

example as revealed by ramped pyrolysis/oxidation (Rosenheim and Galy, 2010; Rosenheim et al., 2013; Hemingway et al., 2018).

### 4.3 River Discharge of $\text{POC}_{\text{petro}}$ and $\text{POC}_{\text{biosphere}}$

#### 4.3.1 $\text{POC}_{\text{petro}}$ Yield

$\text{POC}_{\text{petro}}$  discharge is calculated by multiplying the suspended sediment discharge by  $[\text{OC}_{\text{petro}}]$ , which can be estimated by the hyperbolic regression of  $F_{\text{mod}}$  versus  $[\text{OC}_{\text{total}}]$ . Based on this approach,  $\text{POC}_{\text{petro}}$  accounts for  $11.8 \pm 7.0\%$  to  $42.3 \pm 15.3\%$  of the total POC across the study area. When the  $\text{POC}_{\text{petro}}$  discharge is normalized to the catchment area, the annual  $\text{POC}_{\text{petro}}$  yield ranges from  $0.04 \pm 0.02 \text{ tC km}^{-2} \text{ yr}^{-1}$  to  $1.69 \pm 0.56 \text{ tC km}^{-2} \text{ yr}^{-1}$  (Table EA4). In terms of individual stations, the mean  $\text{POC}_{\text{petro}}$  yield varies from  $0.19 \pm 0.11 \text{ tC km}^{-2} \text{ yr}^{-1}$  at station U3 to  $0.85 \pm 0.28 \text{ tC km}^{-2} \text{ yr}^{-1}$  at station U2 (Table 1).  $\text{POC}_{\text{petro}}$  yield increases with the suspended sediment yield (Fig. 6a), in agreement with other observations from mountain rivers where erosion rates are much higher (Hilton et al., 2011) as well as with the global river trend (Galy et al., 2015). As a tectonically active mountain belt, the Longmen Shan is characterized by relatively frequent mass wasting events. Topographic slope is a first order control on mass wasting processes (Burbank et al., 1996; Larsen and Montgomery, 2012) and we find that higher average slope is associated with higher rates of  $\text{POC}_{\text{petro}}$  erosion, albeit not at the 95% confidence level ( $p = 0.06$ ; Fig. 6b). The scatter may result from the limited number of stations studied here, the thresholds in the relationship between erosion rate and slope which relate to the bedrock landsliding process (Ouimet et al., 2009), as well as other factors such as climate that may affect erosional fluxes (Wang et al., 2015; Li et al., 2017).

$[\text{OC}_{\text{petro}}]$  in the Longmen Shan (Table 1) is heterogeneous between the main catchments in bedrocks bed materials, and as inferred from the mixing model, the suspended sediments (Fig. 5). Observed changes in sediment  $[\text{OC}_{\text{petro}}]$  from upstream to downstream in each catchment can be explained by variation in  $[\text{OC}_{\text{petro}}]$  input or by oxidation of petrogenic OC during sediment transfer (Galy et al., 2008; Hilton et al., 2011). In this region, the variable bedrock geology (and range of associated  $[\text{OC}_{\text{petro}}]$ ) makes it difficult to resolve any losses of petrogenic carbon associated with oxidative weathering (Bouchez et al., 2010). Future work could seek to establish the rates and patterns of  $\text{POC}_{\text{petro}}$  oxidation in this mountain range, and

the extent to which it counters biospheric OC discharge, but would require alternative approaches to track and quantify  $\text{POC}_{\text{petro}}$  loss (Hilton et al., 2014).

#### 4.3.2 $\text{POC}_{\text{biosphere}}$ Yields

In the Longmen Shan, the annual  $\text{POC}_{\text{biosphere}}$  yield calculated as the difference between total POC and  $\text{POC}_{\text{petro}}$  yield across the study catchments ranges from  $0.21 \pm 0.04 \text{ tC km}^{-2} \text{ yr}^{-1}$  to  $3.33 \pm 0.57 \text{ tC km}^{-2} \text{ yr}^{-1}$ , and these yields are broadly correlated with annual suspended sediment yield (Table EA4; Fig. 7a). The average  $\text{POC}_{\text{biosphere}}$  of individual stations during 2006 – 2012 ranged from  $0.84 \pm 0.21 \text{ tC km}^{-2} \text{ yr}^{-1}$  at station D1 to  $1.49 \pm 0.27 \text{ tC km}^{-2} \text{ yr}^{-1}$  at station U1 (Table 1). When the annual  $\text{POC}_{\text{biosphere}}$  yields calculated here are compared to global compilations, the data from the Min Jiang catchments are consistent with the idea that  $\text{POC}_{\text{biosphere}}$  yield is primary controlled by erosion (Fig. 7a and b; Galy et al., 2015).

In more detail, the upper Min Jiang catchments have  $\text{POC}_{\text{biosphere}}$  yields which are towards the lower end of published data for their suspended sediment yields (Fig. 7). Runoff can enhance erosion of sediment and  $\text{POC}_{\text{biosphere}}$  from hillslopes and increase the transport capacity of rivers downstream (Hilton, 2017). Higher runoff results in higher  $\text{POC}_{\text{biosphere}}$  discharge in global mountain rivers (Hilton, 2017). The data from individual stations from the Longmen Shan agree with these patterns, having relatively low annual runoff, which results in lower  $\text{POC}_{\text{biosphere}}$  yield (Fig. 7b).

The normalized maximum daily runoff – a metric derived by dividing the maximum runoff by the annual average runoff as a measure of runoff intensity – also strongly controls the  $\text{POC}_{\text{biosphere}}$  yield in the study area ( $p < 0.01$ ; Fig. 7c). This observation is consistent with the evacuation of earthquake-triggered landslide debris, which is best explained by high intensity runoff events (Wang et al., 2015; Li et al., 2017). It appears that climate regulates the export of  $\text{POC}_{\text{biosphere}}$  erosion in the Longmen Shan, with intense precipitation driving erosion and supply to rivers (Fig. 7c). Depending on the magnitude of the fluxes involved and the long-term fate of  $\text{POC}_{\text{biosphere}}$ , this climate dependency could represent a stabilizing feedback in the Earth System: an increase in atmospheric  $\text{CO}_2$  concentrations and warmer/wetter world could increase the erosional export of  $\text{POC}_{\text{biosphere}}$  to rivers. The climate regulation of  $\text{POC}_{\text{biosphere}}$  export works in tandem with tectonic uplift and large

earthquakes in mobilizing large quantities of  $\text{POC}_{\text{biosphere}}$  for erosion in Longmen Shan.

## 5. Conclusions

Mountain rivers erode and transport a significant amount of organic carbon from sedimentary rocks and the terrestrial biosphere. We quantified the flux of these different sources of POC in the upper Min Jiang, at the eastern margin of the Tibetan Plateau, using the isotopic composition of organic carbon in suspended sediment and river bed material samples, soils, bedrock, and vegetation. Radiocarbon content and an end-member mixing model were used to estimate the mean age of  $\text{POC}_{\text{biosphere}}$  in rivers, which ranges from modern to  $>1620 \pm 980/-870$   $^{14}\text{C}$  years. The mean biospheric OC  $^{14}\text{C}$  ages were oldest in two of the upstream catchments which drain the highest elevations at the eastern margin of the Tibetan Plateau (at  $\pm 1\text{SE}$  confidence intervals). However, the uncertainty of the mixing model precludes detailed assessment of the downstream change of biospheric OC  $^{14}\text{C}$  age at 95% confidence intervals.

The end-member mixing model was also used to calculate the petrogenic organic carbon concentrations. Annual  $\text{POC}_{\text{petro}}$  yields from each station were calculated by multiplying calculated concentrations by the suspended sediment yield and ranged from  $0.04 \pm 0.02 \text{ tC km}^{-2} \text{ yr}^{-1}$  from  $1.69 \pm 0.56 \text{ tC km}^{-2} \text{ yr}^{-1}$ . Across the catchments studied here, these yields are broadly correlated with the suspended sediment yield (Fig. 6a), indicating the important role of physical erosion in  $\text{POC}_{\text{petro}}$  erosion. The isotopic composition of  $\text{POC}_{\text{petro}}$  in parts of the upper Min Jiang distinguishes this system from others, with the mean  $\delta^{13}\text{C}_{\text{org}}$  values of river bed materials reaching  $\sim -16\text{‰}$  in one catchment. This  $^{13}\text{C}$  enrichment of  $\text{POC}_{\text{petro}}$  could result from metamorphic processes. The variability in the concentration of  $\text{POC}_{\text{petro}}$  between different catchments, likely resulting from lithological heterogeneity, obscures tracking any potential losses of  $\text{POC}_{\text{petro}}$  during weathering.

Our mixing analysis suggests that 58% – 88% of the POC carried by the upper Min Jiang derives from  $\text{POC}_{\text{biosphere}}$ . The annual  $\text{POC}_{\text{biosphere}}$  yield across the study catchments ranges from  $0.21 \pm 0.04 \text{ tC km}^{-2} \text{ yr}^{-1}$  to  $3.33 \pm 0.57 \text{ tC km}^{-2} \text{ yr}^{-1}$ , which is set by the intense runoff events (Fig. 7c). An increased frequency of intense rainfall events in the future could lead to enhanced erosion of  $\text{POC}_{\text{biosphere}}$  from high

elevations, where the rate of warming is likely to be amplified (Mountain Research Initiative EDW Working Group, 2015) and carbon stocks are large in high elevation soils (Ding et al., 2016). Our study calls for future work to constrain the age of  $\text{POC}_{\text{biosphere}}$  and its fate, alongside that of  $\text{POC}_{\text{petro}}$ , following erosion from the eastern Tibetan Plateau.

### Acknowledgements:

Funding for this research was provided by Chinese Academy of Sciences programs (QYZDJ-SSW-DQC033, 132B61KYSB20170008) and NSFC (41773149) to Z.J., Chinese Academy of Sciences YIS Fellowships to A.J.W. and R.G.H., and a COFUND Junior Research Fellowship of Durham University to J.W. R.G.H. was also supported by a European Research Council Starting Grant (ERC-StG, 678779, ROC-CO2). We thank F. Davies, N. Tunstall, A. George, A. Hayton, and K. Melvin for assistance in the laboratory, L. Chen for assistance in sample collection, and X. Feng for discussions during manuscript preparation. We thank J. Hemingway and three anonymous referees for insightful comments that improved the manuscript.

### References:

- Andreae, M. O. (1974) Chemical and stable isotope composition of the high grade metamorphic rocks from the Arendal area, Southern Norway. *Contrib. Mineral. Petrol.* **47**, 299-316.
- Battin, T. J., Kaplan, L. A., Findlay, S., Hopkinson, C. S., Marti, E., Packman, A. I., Newbold, J. D. and Sabater, F. (2008) Biophysical controls on organic carbon fluxes in fluvial networks. *Nat. Geosci.* **1**, 95-100.
- Berhe, A. A., Harte, J., Harden, J. W. and Torn, M. S. (2007) The significance of the erosion-induced terrestrial carbon sink. *BioScience* **57**, 337-346.
- Berner, R. A. (1982) Burial of organic carbon and pyrite sulfur in the modern ocean: its geochemical and environmental significance. *Am. J. Sci.* **282**, 451-473.
- Blair, N. E., Leithold, E. L., Ford, S. T., Peeler, K. A., Holmes, J. C. and Perkey, D. W. (2003) The persistence of memory: the fate of ancient sedimentary organic carbon in a modern sedimentary system. *Geochim. Cosmochim. Acta* **67**, 63-73.
- Bouchez, J., Beyssac, O., Galy, V., Gaillardet, J., France-Lanord, C., Maurice, L. and Moreira-Turcq, P. (2010) Oxidation of petrogenic organic carbon in the Amazon floodplain as a source of atmospheric  $\text{CO}_2$ . *Geology* **38**, 255-258.
- Burbank, D. W., Leland, J., Fielding, E. and Anderson, R. S. (1996) Bedrock incision, rock uplift and threshold hillslopes in the northwestern Himalayas. *Nature* **379**, 505-510.
- Burchfiel, B. C., Chen, Z., Liu, Y. and Royden, L. H. (1995) Tectonics of the Longmen Shan and Adjacent Regions, Central China. *Int. Geol. Rev.* **37**, 661-735.
- Burchfiel, B. C., Royden, L. H., Van der Hilst, R. D., Hager, B. H., Chen, Z., King, R. W., Li, C., Lü, J., Yao, H. and Kirby, E. (2008) A geological and geophysical context for the Wenchuan earthquake of 12 May 2008, Sichuan, People's Republic of China. *GSA Today* **18**, doi: 10.1130/GSATG18A.1.

- Chen, S. F. and Wilson, C. J. L. (1996) Emplacement of the Longmen Shan Thrust—Nappe Belt along the eastern margin of the Tibetan Plateau. *J. Struct. Geol.* **18**, 413-430.
- China Geological Survey (2004), China Geological Base Map and Instructions (1:2,500,000), (ed. K. Huang). SinoMaps Press, Beijing.
- Clark, K. E., Hilton, R. G., West, A. J., Malhi, Y., Gröcke, D. R., Bryant, C. L., Ascough, P. L., Robles Caceres, A. and New, M. (2013) New views on “old” carbon in the Amazon River: Insight from the source of organic carbon eroded from the Peruvian Andes. *Geochem. Geophys. Geosyst.* **14**, 1644-1659.
- Clark, K. E., Hilton, R. G., West, A. J., Robles Caceres, A., Gröcke, D. R., Marthews, T. R., Ferguson, R. I., Asner, G. P., New, M. and Malhi, Y. (2017) Erosion of organic carbon from the Andes and its effects on ecosystem carbon dioxide balance. *J. Geophys. Res.: Biogeosci.* **122**, 449-469.
- Cui, X., Liu, S. and Wei, X. (2012) Impacts of forest changes on hydrology: a case study of large watersheds in the upper reaches of Minjiang River watershed in China. *Hydrol. Earth Syst. Sci.* **16**, 4279-4290.
- Densmore, A. L., Ellis, M. A., Li, Y., Zhou, R., Hancock, G. S. and Richardson, N. (2007) Active tectonics of the Beichuan and Pengguan faults at the eastern margin of the Tibetan Plateau. *Tectonics* **26**, TC405, doi:10.1029/2006TC001987.
- Ding, J., Li, F., Yang, G., Chen, L., Zhang, B., Liu, L., Fang, K., Qin, S., Chen, Y., Peng, Y., Ji, C., He, H., Smith, P. and Yang, Y. (2016) The permafrost carbon inventory on the Tibetan Plateau: a new evaluation using deep sediment cores. *Global. Change Biol.* **22**, 2688-2701.
- Editorial Committee for Vegetation of China, Chinese Academy of Sciences. (2007) The Vegetation Map of the People's Republic of China (1:1000000). Geological Publishing House, Beijing.
- Feng, X., Vonk, J. E., van Dongen, B. E., Gustafsson, Ö., Semiletov, I. P., Dudarev, O. V., Wang, Z., Montluçon, D. B., Wacker, L. and Eglinton, T. I. (2013) Differential mobilization of terrestrial carbon pools in Eurasian Arctic river basins. *Proc. Natl. Acad. Sci. U.S.A.* **110**, 14168-14173.
- France-Lanord, C. and Derry, L. A. (1997) Organic carbon burial forcing of the carbon cycle from Himalayan erosion. *Nature* **390**, 65-67.
- Galy, A. and France-Lanord, C. (2001) Higher erosion rates in the Himalaya: Geochemical constraints on riverine fluxes. *Geology* **29**, 23-26.
- Galy, V. and Eglinton, T. I. (2011) Protracted storage of biospheric carbon in the Ganges–Brahmaputra basin. *Nat. Geosci.* **4**, 843-847.
- Galy, V., France-Lanord, C., Beyssac, O., Faure, P., Kudrass, H. and Palhol, F. (2007) Efficient organic carbon burial in the Bengal fan sustained by the Himalayan erosional system. *Nature* **450**, 407-410.
- Galy, V., Beyssac, O., France-Lanord, C. and Eglinton, T. I. (2008a) Recycling of graphite during Himalayan erosion: a geological stabilization of carbon in the crust. *Science* **322**, 943-945.
- Galy, V., France-Lanord, C. and Lartiges, B. (2008b). Loading and fate of particulate organic carbon from the Himalaya to the Ganga–Brahmaputra delta. *Geochim. Cosmochim. Acta*, **72**, 1767-1787.
- Galy, V., Peucker-Ehrenbrink, B. and Eglinton, T. I. (2015) Global carbon export from the terrestrial biosphere controlled by erosion. *Nature* **521**, 204-207.
- Godard, V., Lavé, J., Carcaillet, J., Cattin, R., Bourlès, D. and Zhu, J. (2010) Spatial distribution of denudation in Eastern Tibet and regressive erosion of plateau margins. *Tectonophysics* **491**, 253-274.
- Hara, E. (2016). Earthquake Driven Erosion of Organic Carbon. MSc thesis, University of Southern California.
- Hayes, J. M., Strauss, K. and Kaufman, A. J. (1999) The abundance of <sup>13</sup>C in marine organic matter and isotopic fractionation in the global biogeochemical cycle of carbon during the past 800 Ma. *Chem. Geol.* **161**, 103-125.

- Hemingway, J. D., Hilton, R. G., Hovius, N., Eglinton, T. I., Haghypour, N., Wacker, L., Chen, M.C. and Galy, V. (2018). Microbial oxidation of lithospheric organic carbon in rapidly eroding tropical mountain soils. *Science*, **360**, 209-212.
- Hilton, R. G. (2017) Climate regulates the erosional carbon export from the terrestrial biosphere. *Geomorphology* **277**, 118-132.
- Hilton, R. G., Galy, A., Hovius, N., Chen, M. -C., Horng, M. -J. and Chen, H. (2008a) Tropical-cyclone-driven erosion of the terrestrial biosphere from mountains. *Nat. Geosci.* **1**, 759-762.
- Hilton, R. G., Galy, A. and Hovius, N. (2008b) Riverine particulate organic carbon from an active mountain belt: Importance of landslides. *Glob. Biogeochem. Cycles* **22**, GB1017, doi:10.1029/2006GB002905.
- Hilton, R. G., Galy, A., Hovius, N., Horng, M. -J. and Chen, H. (2010) The isotopic composition of particulate organic carbon in mountain rivers of Taiwan. *Geochim. Cosmochim. Acta* **74**, 3164-3181.
- Hilton, R. G., Galy, A., Hovius, N., Horng, M. -J. and Chen, H. (2011) Efficient transport of fossil organic carbon to the ocean by steep mountain rivers: An orogenic carbon sequestration mechanism. *Geology* **39**, 71-74.
- Hilton, R. G., Gaillardet, J., Calmels, D. and Birck, J. -L. (2014) Geological respiration of a mountain belt revealed by the trace element rhenium. *Earth Planet. Sci. Lett.* **403**, 27-36.
- Hilton, R. G., Galy, V., Gaillardet, J., Dellinger, M., Bryant, C., O'Regan, M., Gröcke, D. R., Coxall, H., Bouchez, J. and Calmels, D. (2015) Erosion of organic carbon in the Arctic as a geological carbon dioxide sink. *Nature* **524**, 84-87.
- Hoefs, J. and Frey, M. (1976) The isotopic composition of carbonaceous matter in a metamorphic profile from the Swiss Alps. *Geochim. Cosmochim. Acta* **40**, 945-951.
- Kao, S. -J., Hilton, R. G., Selvaraj, K., Dai, M., Zehetner, F., Huang, J. -C., Hsu, S. -C., Sparkes, R., Liu, J. T., Lee, T. -Y., Yang, J. -Y. T., Galy, A., Xu, X. and Hovius, N. (2014) Preservation of terrestrial organic carbon in marine sediments offshore Taiwan: mountain building and atmospheric carbon dioxide sequestration. *Earth Surf. Dynam.* **2**, 127-139.
- Komada, T., Druffel, E. R. and Trumbore, S. E. (2004) Oceanic export of relict carbon by small mountainous rivers. *Geophys. Res. Lett.* **31**, L07504, doi:10.1029/2004GL019512, .
- Körner, C., Farquhar, G. D. and Roksandic, Z. (1988) A global survey of carbon isotope discrimination in plants from high altitude. *Oecologia* **74**, 623-632.
- Larsen, I. J. and Montgomery, D. R. (2012) Landslide erosion coupled to tectonics and river incision. *Nat. Geosci.* **5**, 468-473.
- Leithold, E. L., Blair, N. E. and Perkey, D. W. (2006) Geomorphologic controls on the age of particulate organic carbon from small mountainous and upland rivers. *Glob. Biogeochem. Cycles* **20**, GB3022, doi:10.1029/2005GB002677.
- Li, G., West, A. J., Densmore, A. L., Jin, Z., Parker, R. N. and Hilton, R. G. (2014) Seismic mountain building: Landslides associated with the 2008 Wenchuan earthquake in the context of a generalized model for earthquake volume balance. *Geochem. Geophys. Geosyst.* **15**, 833-844.
- Li, G., West, A. J., Densmore, A. L., Jin, Z., Zhang, F., Wang, J., Clark, M. and Hilton, R. G. (2017) Earthquakes drive focused denudation along a tectonically active mountain front. *Earth Planet. Sci. Lett.* **472**, 253-265.
- Liu-Zeng, J., Wen, L., Oskin, M. and Zeng, L. (2011) Focused modern denudation of the Longmen Shan margin, eastern Tibetan Plateau. *Geochem. Geophys. Geosyst.* **12**, Q11007, doi:10.1029/2011GC003652.
- Marwick, T. R., Tamooch, F., Teodoru, C. R., Borges, A. V., Darchambeau, F. and Bouillon, S. (2015) The age of river-transported carbon: A global perspective. *Glob. Biogeochem. Cycles* **29**, 122-137.

- Mayorga, E., Aufdenkampe, A. K., Masiello, C. A., Krusche, A. V., Hedges, J. I., Quay, P. D., Richey, J. E. and Brown, T. A. (2005) Young organic matter as a source of carbon dioxide outgassing from Amazonian rivers. *Nature* **436**, 538-541.
- Milliman, J. D. and Farnsworth, K. L. (2011) River discharge to the coastal ocean: a global synthesis. Cambridge University Press, Cambridge.
- Ministry of Water Resources of China (2007) Code for Measurements of Suspended Sediment in Open Channels (GB50159–92). China Planning Press, Beijing (in Chinese).
- Mountain Research Initiative EDW Working Group. (2015) Elevation-dependent warming in mountain regions of the world. *Nat. Clim. Change* **5**, 424-430.
- Ouimet, W. B. (2010) Landslides associated with the May 12, 2008 Wenchuan earthquake: Implications for the erosion and tectonic evolution of the Longmen Shan. *Tectonophysics* **491**, 244-252.
- Ouimet, W. B., Whipple, K. X. and Granger, D. E. (2009) Beyond threshold hillslopes: Channel adjustment to base-level fall in tectonically active mountain ranges. *Geology* **37**, 579-582.
- Parker, R. N., Densmore, A. L., Rosser, N. J., de Michele, M., Li, Y., Huang, R., Whadcoat, S. and Petley, D. N. (2011) Mass wasting triggered by the 2008 Wenchuan earthquake is greater than orogenic growth. *Nat. Geosci.* **4**, 449-452.
- Petsch, S. T., Berner, R. A. and Eglinton, T. I. (2000) A field study of the chemical weathering of ancient sedimentary organic matter. *Org. Geochem.* **31**, 475-487.
- Ponton, C., West, A. J., Feakins, S. J. and Galy, V. (2014) Leaf wax biomarkers in transit record river catchment composition. *Geophys. Res. Lett.* **41**, 6420-6427.
- Robert, A., Pubellier, M., de Sigoyer, J., Vergne, J., Lahfid, A., Cattin, R., Findling, N. and Zhu, J. (2010) Structural and thermal characters of the Longmen Shan (Sichuan, China). *Tectonophysics* **491**, 165-173.
- Rosenheim, B. E. and Galy, V. (2012), Direct measurement of riverine particulate organic carbon age structure, *Geophys. Res. Lett.* **39**, L19703, doi:10.1029/2012GL052883.
- Rosenheim, B. E., Roe, K. M., Roberts, B. J., Kolker, A. S., Allison, M. A. and Johannesson, K. H. (2013). River discharge influences on particulate organic carbon age structure in the Mississippi/Atchafalaya River System. *Glob. Biogeochem. Cycles* **27**, 154-166.
- Schwab, V., Spangenberg, J. E. and Grimalt, J. O. (2005) Chemical and carbon isotopic evolution of hydrocarbons during prograde metamorphism from 100°C to 550°C: Case study in the Liassic black shale formation of Central Swiss Alps. *Geochim. Cosmochim. Acta* **69**, 1825-1840.
- Tao, S., Eglinton, T. I., Montluçon, D. B., McIntyre, C. and Zhao, M. (2015) Pre-aged soil organic carbon as a major component of the Yellow River suspended load: Regional significance and global relevance. *Earth Planet. Sci. Lett.* **414**, 77-86.
- Wang, J., Jin, Z., Hilton, R. G., Zhang, F., Densmore, A. L., Li, G. and West, A. J. (2015) Controls on fluvial evacuation of sediment from earthquake-triggered landslides. *Geology* **43**, 115-118.
- Wang, J., Jin, Z., Hilton, R. G., Zhang, F., Li, G., Densmore, A. L., Gröcke, D. R., Xu, X. and West, A. J. (2016) Earthquake-triggered increase in biospheric carbon export from a mountain belt. *Geology* **44**, 471-474.
- Xian, J., Zhang, Y., Hu, T., Wang, K. and Yang, H. (2009) Carbon stock and allocation of five restoration ecosystems in subalpine coniferous forest zone in Western Sichuan Province, Southwest China. *Acta Ecol. Sin.* **29**, 51-55.
- Xu, W., Ruhl, M., Jenkyns, H. C., Hesselbo, S. P., Riding, J. B., Selby, D., Naafs, B. D. A., Weijers, J. W., Pancost, R. D., Tegelaar, E. W. and Idiz, E. F. (2017) Carbon sequestration in an expanded lake system during the Toarcian oceanic anoxic event. *Nat. Geosci.* **10**, 129-134.
- Yue, Y., Ni, J., Ciais, P., Piao, S., Wang, T., Huang, M., Borthwick, A. G., Li, T., Wang, Y. and Chappell, A. (2016) Lateral transport of soil carbon and land – atmosphere CO<sub>2</sub> flux induced by water erosion in China. *Proc. Natl. Acad. Sci. U.S.A.* **113**, 6617-6622.

- Zhang, G. (2008) Forest Carbon Storage Dynamics at the Upper stream of Minjiang River. Ph.D. thesis, Chinese Academy of Forest (in Chinese with English abstract).
- Zhang, Y., Duan, Z. and Dou, J. (2005) Comparison of climate characteristics between a dry-warm valley in upper reaches of Min River and a dry-hot valley of Yuanjiang River. *Resources and Environment in the Yangtze Basin* **14**, 76-82 (in Chinese with English abstract).

### Figure Captions:

Figure 1. The upper Min Jiang river basin in the Longmen Shan range, on the eastern margin of the Tibetan Plateau. (a) 6 gauging stations (white stars; U1 = Heishui station, D1= Shaba station on the Heishui River; U2 = Zagunao station, D2 = Sangping station on the Zagunao River; U3 = Zhenjiangguan station, D3 = Weizhou station on the Min Jiang) overlain on topography from the shuttle Radar Topographic Mission (SRTM) digital elevation model at 30 x 30 m resolution. The red lines are the faults which ruptured in the 2008 Wenchuan earthquake. (b) Bedrock type and bedrock and soil sampling sites (grey circle = bedrock sampling, triangle = soil sampling). Geology is modified from a 1: 2,500,000 China Geological Base Map (China Geological Survey, 2004). (c) Vegetation type (Editorial Committee for Vegetation of China, Chinese Academy of Sciences, 2007), showing vegetation (green triangle) and river bed material (yellow circle) sampling sites.

Figure 2. Relationships between suspended-sediment concentration (SSC,  $\text{g L}^{-1}$ ) and total POC concentration ( $[\text{POC}_{\text{total}}]$ ,  $\text{mg L}^{-1}$ ) for the upper Min Jiang. The open symbols are the upstream stations (green = U1, blue = U2, pink = U3) and the corresponding filled symbols are the downstream stations (stations D1, D2, D3). The lines show orthogonal distance regressions through log-transformed data at the upstream stations (dashed lines) and at the downstream stations (solid lines) with corresponding colors.

Figure 3. Stable carbon isotopic composition ( $\delta^{13}\text{C}_{\text{org}}$ ) of POC versus one over the total organic carbon content ( $1/[\text{OC}_{\text{total}}]$ ) for the (a) upstream and (b) downstream gauging stations. The symbols are the same as in Figure 2. Error bars show  $\pm 1\sigma$  standard deviation. The black rectangles in each panel show the mean compositions of the vegetation collected over all catchments. The triangles with labels O<sub>H</sub>, A, and B-C show the compositions of the respective soil horizons collected throughout all the catchment.

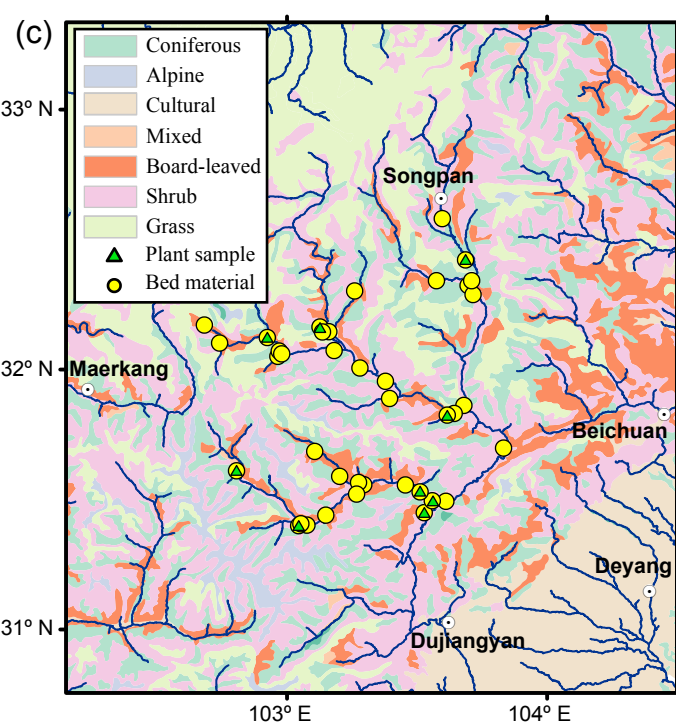
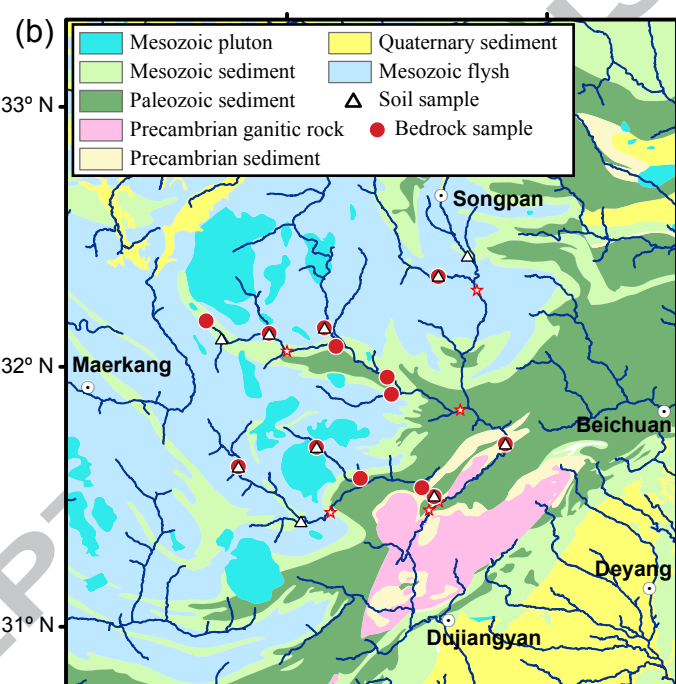
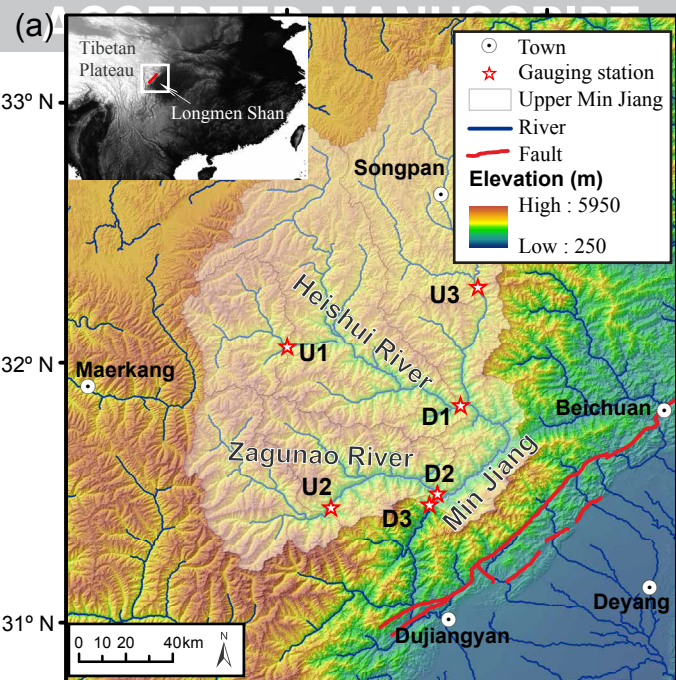
Figure 4. Radiocarbon activity of POC reported as fraction modern ( $F_{\text{mod}}$ ) versus stable carbon isotopic composition ( $\delta^{13}\text{C}_{\text{org}}$ ) and  $1/[\text{OC}_{\text{total}}]$  for the upstream (a and c) and downstream (b and d) gauging stations. The squares show the mean  $\delta^{13}\text{C}_{\text{org}}$  values of the river bed materials collected within each catchment, which represent rock-derived  $\text{POC}_{\text{petro}}$  sources. The boxes above the x-axes show the ranges of  $\delta^{13}\text{C}_{\text{org}}$  and  $1/[\text{OC}_{\text{total}}]$  where O<sub>H</sub>, A, and B-C refer to the respective soil horizons and

C3 to the C3 vegetation samples collected throughout the study area, all of which represent  $\text{POC}_{\text{biosphere}}$  sources with unknown  $F_{\text{mod}}$ .

Figure 5. The radiocarbon carbon activity of biospheric carbon,  $F_{\text{mod-bio}}$ , and the petrogenic organic carbon concentration,  $[\text{OC}_{\text{petro}}]$ , calculated by hyperbolic orthogonal distance regression. (a)-(c)  $F_{\text{mod}}$  versus  $[\text{OC}_{\text{total}}]$  at each station. The open symbols are the upstream stations and the corresponding filled symbols are the downstream stations. The circles in each panel show the data of suspended sediment samples. The triangles in panel (b) show the data of bed materials. The triangles in panels (a) and (c) show the mean compositions of bed materials collected at each catchment with assumption  $F_{\text{mod}} = 0.04 \pm 0.02$ , the mean  $F_{\text{mod}}$  of the two bed material samples showed on panel (b). The dashed and solid lines are the orthogonal distance regression best-fit solutions to the upstream and downstream data, respectively. The best fit solutions minimize the residual error between measured and predicted  $F_{\text{mod}}$  values. The shaded region around each line is the propagated  $\pm 1\text{SE}$  uncertainty.

Figure 6.  $\text{POC}_{\text{petro}}$  yield in the upper Min Jiang. (a) Annual  $\text{POC}_{\text{petro}}$  yield as a function of suspended sediment yield, together with data from global compilations by Galy et al. (2015) and Hilton (2017) for comparison. (b) Average  $\text{POC}_{\text{petro}}$  yield of individual stations in this study as a function of mean catchment slope. The mean catchment slope was calculated based on the SRTM digital elevation model at 30 x 30 m resolution.

Figure 7. Annual  $\text{POC}_{\text{biosphere}}$  yield in the upper Min Jiang as a function of (a) suspended sediment yield, (b) annual runoff, and (c) maximum daily runoff normalized to the mean runoff of 2006 – 2012. The black lines in (a) and (c) are the orthogonal distance regression best-linear-fit to suspended sediment samples at all stations of this study. Also shown in panels (a) and (b) are data from global compilations by Galy et al. (2015) and Hilton (2017) for comparison (but not included in regression in (a)).

**Figure 1**

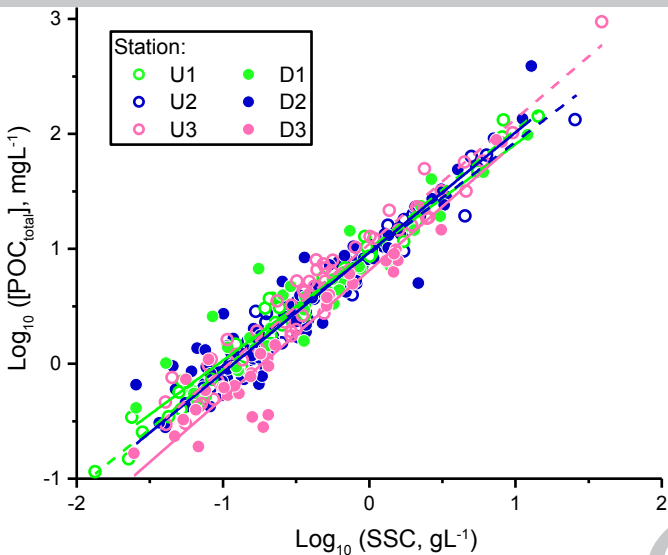
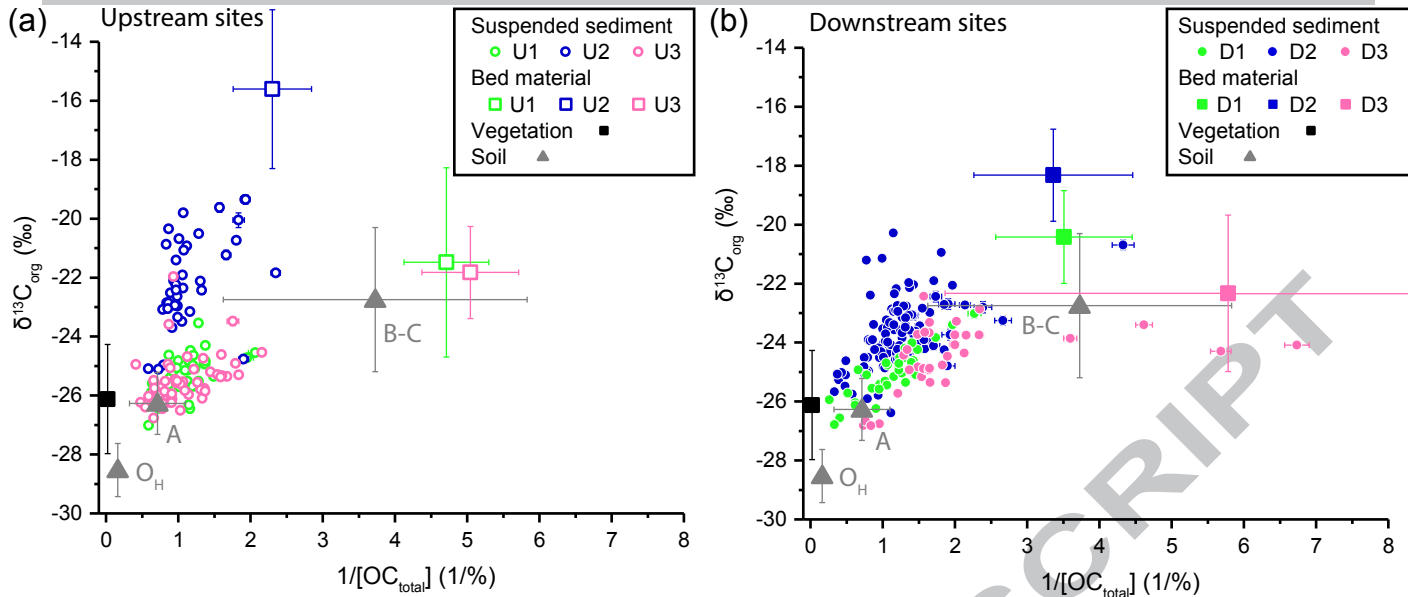
**Figure2****ACCEPTED MANUSCRIPT**

Figure 3

ACCEPTED MANUSCRIPT



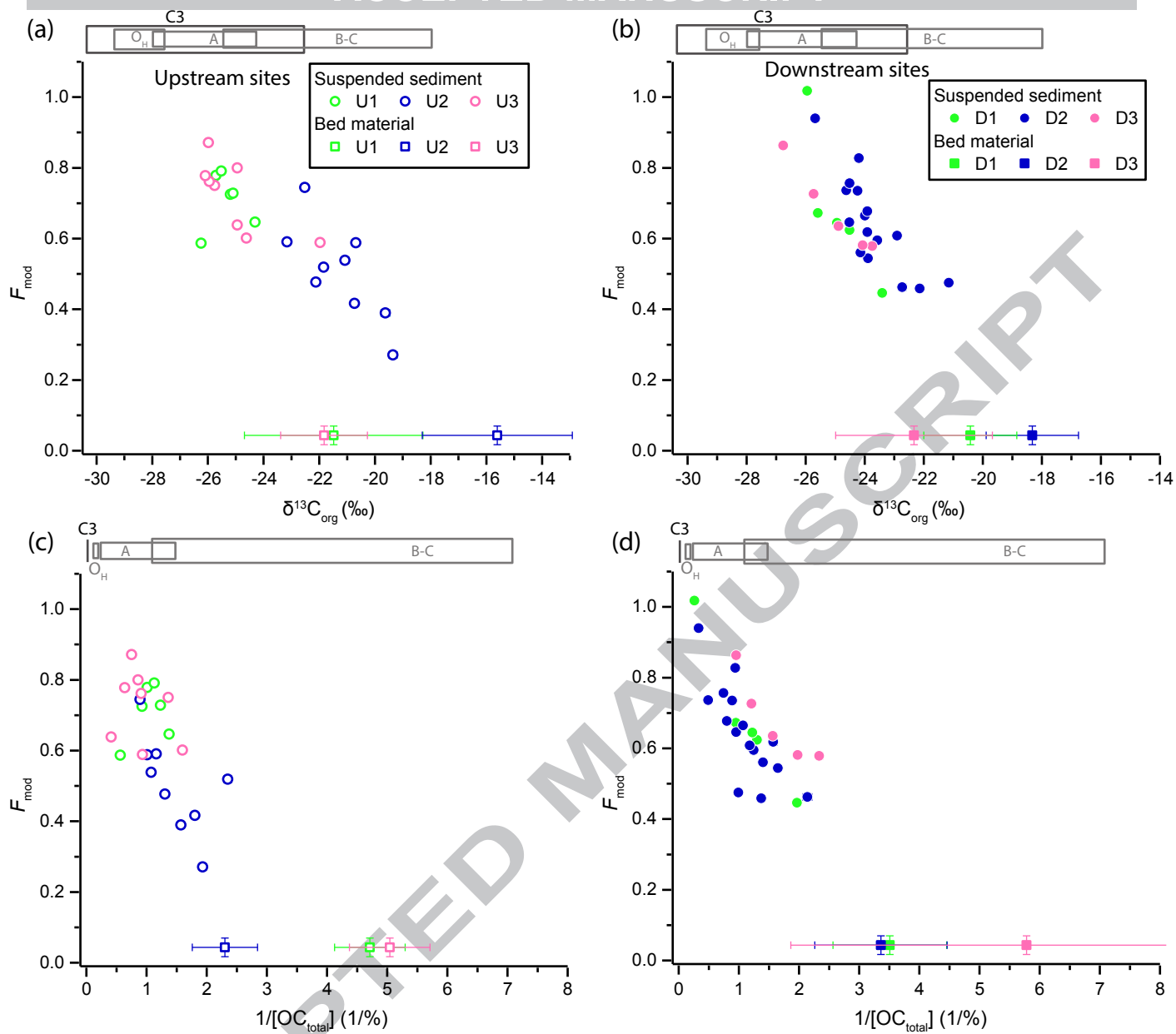
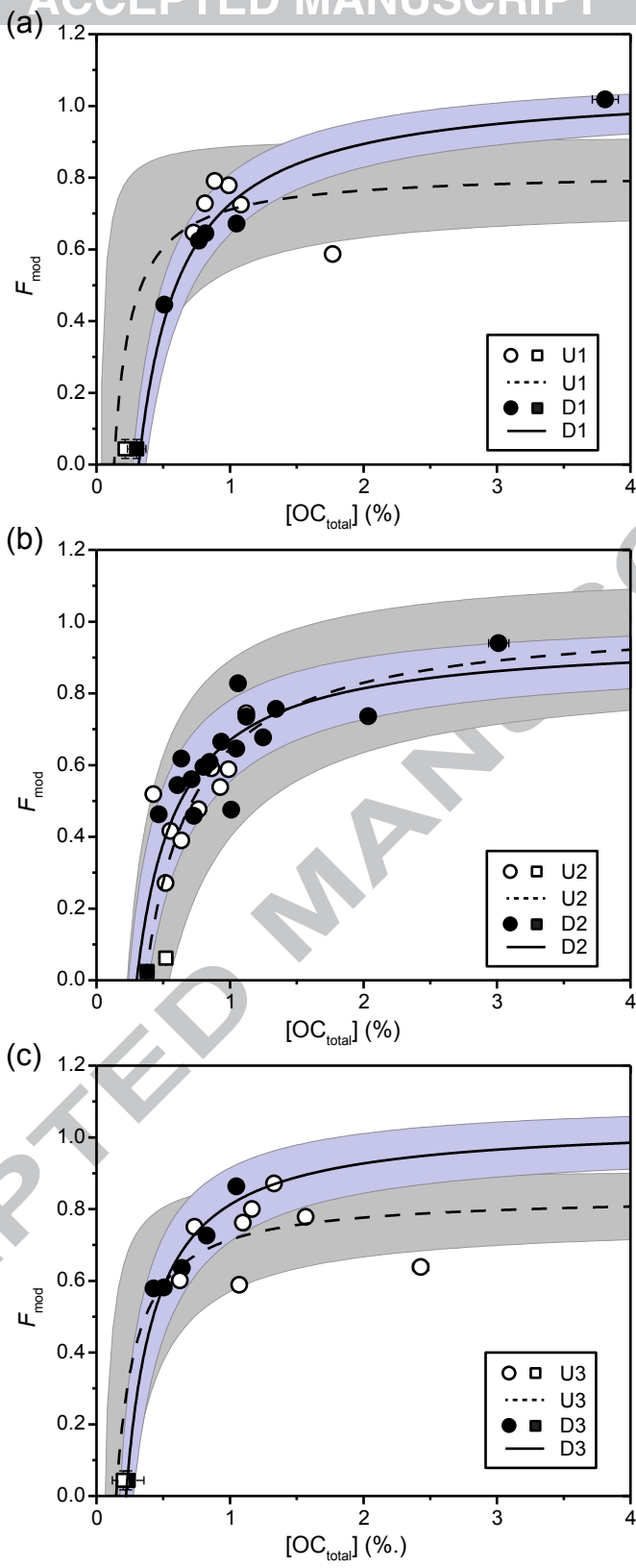


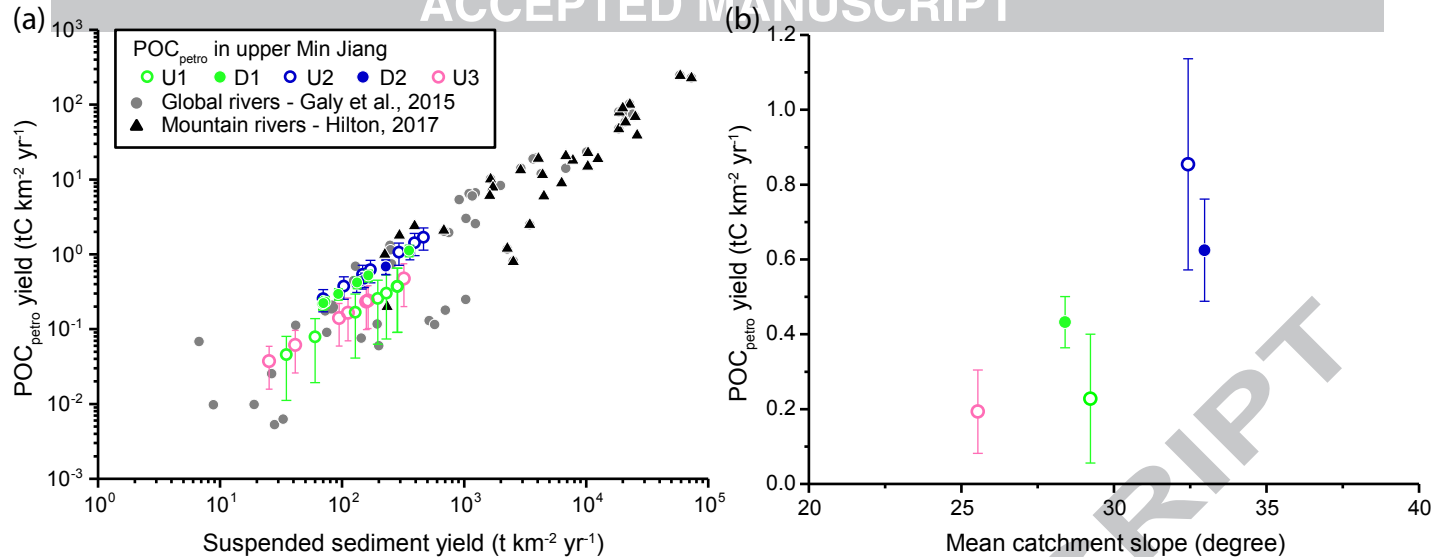
Figure 5

ACCEPTED MANUSCRIPT



**Figure 6**

ACCEPTED MANUSCRIPT



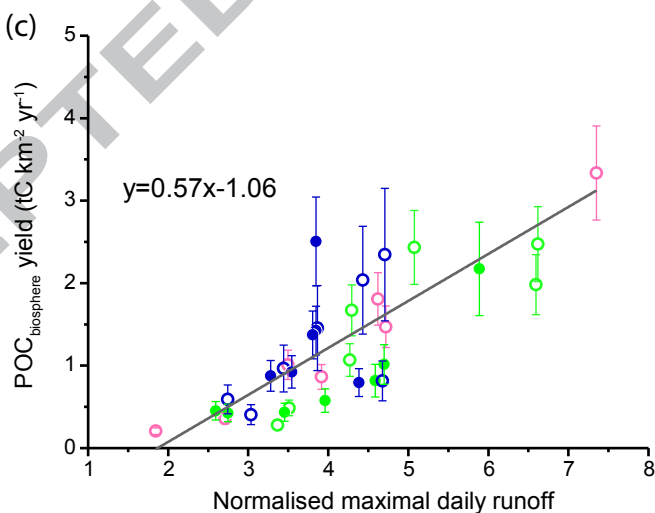
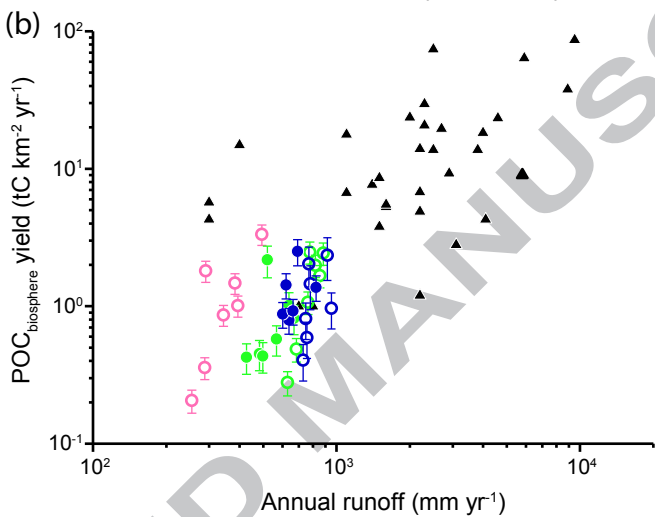
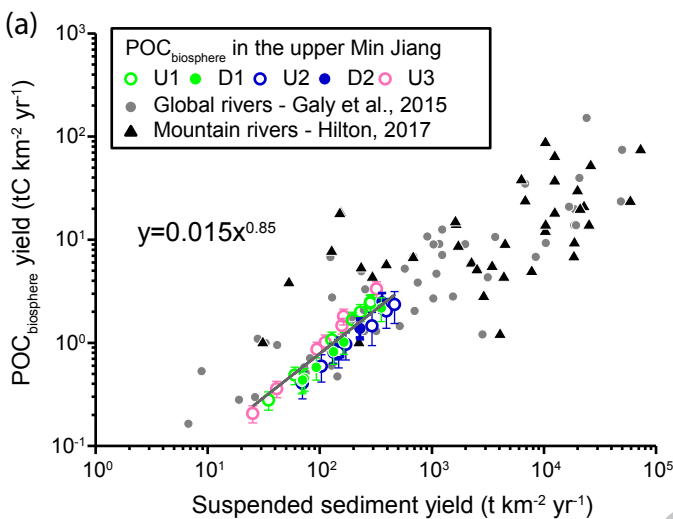


Table 1

Characteristics of gauging stations in the upper Min Jiang and estimates of sediment and POC yield at each station.

River	Heishui tributary		Zagunao tributary		Min Jiang main stream	
Gauging station	Heishui (U1)	Shaba (D1)	Zagunao (U2)	Sangping (D2)	Zhenjiangguan (U3)	Weizhou (D3)
Location	N 32°03'39" E 102°59'52"	N 31°49'53" E 103°39'38"	N 31°26'24" E 103°10'00"	N 31°29'42" E 103°34'36"	N 32°17'21" E 103°44'00"	N 31°26'58" E 103°32'42"
Catchment area (km <sup>2</sup> )	1720	7231	2404	4629	4486	18870
Mean catchment elevation (min–max range) (m)	3851 (2305–5277)	3616 (1710–5277)	3864 (1856–5560)	3618 (1423–5560)	3626 (2460–5510)	3539 (1423–5560)
Mean slope ( $\pm 1\sigma$ , deg)	29.2 $\pm$ 10.6	28.4 $\pm$ 11.2	32.4 $\pm$ 11.2	33.0 $\pm$ 11.3	25.5 $\pm$ 10.2	29.3 $\pm$ 11.4
Annual runoff (mm yr <sup>-1</sup> )	773	543	808	673	350	NA
Suspended sediment yield (t km <sup>-2</sup> yr <sup>-1</sup> ) <sup>a</sup>	174 $\pm$ 17	137 $\pm$ 10	235 $\pm$ 24	208 $\pm$ 21	131 $\pm$ 13	NA
[OC <sub>total</sub> ] of bed materials, %	0.21 $\pm$ 0.03	0.30 $\pm$ 0.07	0.45 $\pm$ 0.09	0.32 $\pm$ 0.09	0.20 $\pm$ 0.03	0.24 $\pm$ 0.12
[OC <sub>petro</sub> ], % <sup>b</sup>	0.13 $\pm$ 0.10	0.32 $\pm$ 0.04	0.36 $\pm$ 0.11	0.30 $\pm$ 0.06	0.15 $\pm$ 0.08	0.22 $\pm$ 0.04
$F_{\text{mod-bio}}$ <sup>b</sup>	0.82 $\pm$ 0.09	1.06 $\pm$ 0.05	1.01 $\pm$ 0.14	0.96 $\pm$ 0.06	0.84 $\pm$ 0.08	1.04 $\pm$ 0.06
[OC <sub>bio</sub> ], % <sup>c</sup>	0.84 $\pm$ 0.18	0.62 $\pm$ 0.16	0.54 $\pm$ 0.18	0.62 $\pm$ 0.15	0.94 $\pm$ 0.19	NA
POC <sub>biosphere</sub> yield (tC km <sup>-2</sup> yr <sup>-1</sup> )	1.49 $\pm$ 0.27	0.84 $\pm$ 0.21	1.23 $\pm$ 0.40	1.32 $\pm$ 0.28	1.29 $\pm$ 0.22	NA
POC <sub>petro</sub> yield (tC km <sup>-2</sup> yr <sup>-1</sup> )	0.23 $\pm$ 0.17	0.43 $\pm$ 0.07	0.85 $\pm$ 0.28	0.62 $\pm$ 0.14	0.19 $\pm$ 0.11	NA

<sup>a</sup> average of suspended sediment yield of 2006 to 2012, except for station D2 (2006 to 2011)

<sup>b</sup> calculated by hyperbolic orthogonal distance regression of  $F_{\text{mod}}$  versus [OC<sub>total</sub>]

<sup>c</sup> average of values calculated dividing the POC<sub>biosphere</sub> yield by suspended sediment yield of each year